Memoirs of the Faculty of Science, Kyoto University, Series of Physics, Astrophysics, Geophysics and Chemistry, Vol. XXXVIII, No. 2, Article 6, 1992

Parity Nonconservation in Neutron Radiative Capture Reactions

By

Hirohiko M. SHIMIZU

Department of Physics, Kyoto University, Kyoto 606-01, Japan

(*Received December 28, 1991*)

Abstract

Parity nonconserving effect in neutron-induced nuclear reactions has been investigated in low energy (n, γ) reactions for several p-wave compound resonances. Large asymmetries with respect to the incident neutron helicity (A_L) have been observed in p-wave resonance cross sections for $^{139}La(E_n=0.734eV)$, $^{81}Br(E_n=0.88eV)$, $^{111}Cd(E_n=4.53eV)$, ^{93}Nb $(E_n=35.9, 42.3eV)$, $^{108}Pd(E_n=2.96eV)$ and $^{124}Sn(E_n=62.0eV)$. Obtained results are $A_L=(9.8\pm0.3)\%$, $(2.1\pm0.1)\%$ and $-(1.3^{+0.7}_{-0.4})\%$ for ^{139}La, ^{81}Br and ^{111}Cd target nuclei, respectively, while no sizable helicity dependence has been observed for ^{93}Nb, ^{108}Pd and ^{124}Sn target nuclei. The phenomena are explained as very large enhancement of interference terms between s- and p-wave amplitudes due to the statistical nature of compound states and the difference of centrifugal potential barriers between the two amplitudes. Dependences of resonance cross sections and their asymmetries with respect to the incident neutron helicity on the angle of emitted γ-rays have been measured for ^{139}La and ^{81}Br, and found to be very small. The dependence of A_L on γ-ray energy has been measured for ^{139}La, and has been found to be independent of γ-ray energy within experimental errors. The results show that the large values of A_L are due to parity mixing in the entrance channel.

The $\boldsymbol{\sigma}_n \cdot \hat{\boldsymbol{k}}_\gamma$ correlation term for ^{139}La has been also measured to study parity mixing effects in exit channels.

1 Introduction

The conservation of parity (P) in a physical system is a discrete symmetry under a space reflection. The parity violation has been established to be a nature of the weak interaction since it was introduced by Lee and Yang [1] in 1956, and it was observed experimentally by Wu et al. [2] in 1957. In nucleon-nucleon (N-N) interactions where the strong interaction is dominant, the parity-nonconserving (PNC) effect is very small. An experimental possibility to observe a PNC effect in N-N interactions was first discussed by Wilkinson [3].[1] The total amplitude (f) consists of parity-conserving (PC) part (f_{PC}) and PNC part (f_{PNC}).

$$f = f_{PC} + f_{PNC} \tag{1}$$

The size of f_{PNC} relative to that of f_{PC} is crudely given by the ratio of PC and PNC light-meson-exchange potentials (V_{PC} and V_{PNC}):

[1] He discussed in the context of parity violation in the strong interaction. Blin-Stoyle discussed the PNC effect in N-N interaction due to the weak interaction [4].

$$\alpha_{NN} = \frac{V_{PNC}}{V_{PC}} \sim G_F m_\pi^2 \sim 2 \times 10^{-7} \sim \frac{|f_{PNC}|}{|f_{PC}|}, \tag{2}$$

where G_F and m_π are the Fermi coupling constant and the pion mass, respectively. The absolute square of f is to be observed experimentally.

$$|f|^2 = |f_{PC}|^2 + 2Ref_{PC}f_{PNC}^* + |f_{PNC}|^2 \sim |f_{PC}|^2(1 + 2\alpha_{NN} + \alpha_{NN}^2) \tag{3}$$

He suggested two types of experiments. The first one is the measurement of a pure PNC part $|f_{PNC}|^2$. For example, search for violation of "absolute" selection rules which are imposed by parity-conservation belongs to this type. The second one is the measurement of $Ref_{PC}f_{PNC}^*$ which is an interference term. The measurement of P-odd correlation terms belongs to this type. Larger PNC effect is expected in the second-type experiment since the PNC effect in the second-type experiment is the order of $\alpha_{NN} \sim 10^{-7}$ while that in the first-type is the order of $\alpha_{NN}^2 \sim 10^{-14}$.

The PNC effect in proton-proton (p-p) interaction has been observed experimentally in the longitudinal asymmetry in p-p scattering which is given as

$$A_L(pp) = \frac{\sigma^+(pp) - \sigma^-(pp)}{\sigma^+(pp) + \sigma^-(pp)}, \tag{4}$$

where $\sigma^+(pp)(\sigma^-(pp))$ is the scattering cross section with incident positive- (negative-) helicity protons. It has been measured at several incident proton energies as listed in Table 1. These results are consistent with theoretical estimations.

Table 1. Longitudinal asymmetry in p-p scattering

incident energy [MeV]	$A_L(pp)$	
15	$-(1.7 \pm 0.8) \times 10^{-7}$	Los Alamos [5]
45	$-(2.3 \pm 0.8) \times 10^{-7}$	SIN [6]
45	$-(1.3 \pm 0.8) \times 10^{-7}$	Berkeley [7]
800	$(2.4 \pm 1.1 \pm 0.1) \times 10^{-7}$	Los Alamos [8]

The first successful observation of a large PNC effect in nuclear process was the measurement of left-right asymmetry of capture γ-rays from an unpolarized ^{113}Cd target induced by transversely polarized incident thermal neutrons from a reactor in 1964 [9]. The left-right asymmetry is a parity violating angular distribution of capture γ-rays (A_γ) which is given as

$$I_\gamma(\theta_{\gamma\sigma_n}) \propto 1 + p_n^T A_\gamma \cos\theta_{\gamma\sigma_n}, \tag{5}$$

where p_n^T and $\theta_{\gamma\sigma_n}$ are the transverse polarization of incident neutrons and the angle between the direction of the incident neutron polarization and the emitted γ-ray momentum. The obtained value is $A_\gamma = -(4.1 \pm 0.8) \times 10^{-4}$. The large PNC effect arises from interference between parity-favored transition (M1) and parity-

unfavored transition (E1) in $^{114}Cd(1^+ \rightarrow 0^+)$. Another large PNC effect was found in the measurement of circular polarization of γ-ray (P_γ) from unpolarized ^{114}Cd nuclei [10]. The obtained value is $P_\gamma = -(6.0 \pm 1.5) \times 10^{-4}$. These types of PNC effect have been studied for a number of nuclei as listed in Table 2. The existence of the large interference term implies that the initial (compound) state or the final state of the γ-ray transition is a parity mixed state. It is natural to assume that the parity is mixed in the initial state, since the level density is much higher in the initial state than in the final state. Therefore, a large PNC effect can be expected also in the entrance channel of the compound state. (The A_γ and P_γ are related to parity mixing in the exit channel of the compound state.)

Table 2. PNC effects in nuclear γ-ray transitions

transition	value	reference
$n + p \rightarrow D(1^+) + \gamma$	$A_\gamma = (0.6 \pm 2.1) \times 10^{-7}$	[11]
	$P_\gamma = -(1.30 \pm 0.45) \times 10^{-6}$	[12]
$^{18}F(0^- \rightarrow 1^+)$	$P_\gamma = -(0.5 \pm 20) \times 10^{-3}$	[13]
$^{19}F(\frac{1}{2}^- \rightarrow \frac{1}{2}^+)$	$A_\gamma = -(18 \pm 9) \times 10^{-5}$	[14]
$^{41}K(\frac{7}{2}^- \rightarrow \frac{3}{2}^+)$	$P_\gamma = (2.0 \pm 0.4) \times 10^{-5}$	[15]
$^{114}Cd(1^+ \rightarrow 0^+)$	$A_\gamma = -(4.0 \pm 0.8) \times 10^{-4}$	[9]
	$P_\gamma = -(6 \pm 1.5) \times 10^{-4}$	[10]
$^{118}Sn(1^+ \rightarrow 0^+)$	$A_\gamma = (4.4 \pm 0.6) \times 10^{-4}$	[16]
	$P_\gamma = (8.5 \pm 1.5) \times 10^{-4}$	[17]
$^{175}Lu(\frac{9}{2}^- \rightarrow \frac{7}{2}^-)$	$P_\gamma = (5.5 \pm 20) \times 10^{-5}$	[18]
$^{180}Hf(8 \rightarrow 6)$	$P_\gamma = -(2.4 \pm 0.3) \times 10^{-3}$	[19]
	$A_\gamma = -(1.7 \pm 0.2) \times 10^{-3}$	[20]
$^{181}Ta(\frac{5}{2}^+ \rightarrow \frac{3}{2}^+)$	$P_\gamma = -(5.2 \pm 0.5) \times 10^{-6}$	[21]

In 1980, a very large PNC effect caused by an interference between two opposite parity amplitudes in the entrance channel was observed in parity violating spin rotation angle of transversely polarized cold neutrons on propagation through ^{117}Sn [22]. The obtained value is $d\phi/dz = (3.7 \pm 0.3) \times 10^{-5}\, rad/cm$. The spin rotation angle corresponds to the real part of the interference term.

The imaginary part of the interference term corresponds to the parity violating asymmetry of a resonance cross section with respect to the helicity of incident neutrons. In this work, very large helicity dependences have been successfully observed in p-wave compound resonances for several target nuclei with incident epithermal neutrons. The ratio of helicity dependent part of the resonance cross section to helicity independent part is referred to as longitudinal asymmetry represented by A_L which is given as

$$A_L = \frac{\sigma_r^+ - \sigma_r^-}{\sigma_r^+ + \sigma_r^-}, \tag{6}$$

where σ_r^+ (σ_r^-) is the resonance cross section induced by incident positive- (negative-) helicity neutrons. In the first experiment carried out at Dubna [23], the longitudinal asymmetry was measured in p-wave resonances for ^{117}Sn, ^{139}La, ^{81}Br

and ^{111}Cd target nuclei, and obtained values are $A_L = 0.45 \pm 0.13\,\%$, $7.3 \pm 0.5\,\%$, $2.4 \pm 0.4\,\%$ and $-0.82 \pm 0.22\,\%$, respectively [23]. Longitudinal asymmetry has been studied in several experiments and measured to be $A_L \sim (10^{-1} \sim 10^{-2})$ in p-wave resonances for several target nuclei [24, 25, 26, 27, 28]. These large PNC effects in compound nucleus are explained to arise from the interference between two opposite parity amplitudes in the entrance channel of the compound state [29, 30, 31]. The parity mixing between two opposite parity amplitudes can be much larger in a compound state than in a direct process, since nucleons have much longer time to interact with each other in a compound state than in a direct process.

The large PNC effect in neutron-nucleus (n-A) interaction introduces a new possibility for testing the time-reversal-invariance (TRI).

The CP-violation was observed in the decay of neutral K mesons by Christenson et al. [37] in 1964, but the origin of CP-violation still remains unknown. If the CPT theorem [38] is true, TRI is broken. A direct measurement of a T-violating effect is very important to study the origin of CP-violation, since the theoretical prediction for T-violation effect in an observable is model dependent because of lack of the knowledge about the origin of CP-violation [39]. No finite T-violating effect has been observed so far in spite of a number of intensive efforts. The experimental upper limits for T-odd amplitudes relative to T-even amplitudes are $\sim 10^{-3}$ for the strong, electromagnetic and weak interactions [40]. The difficulty of the experiments on the TRI test is due to the antiunitarity of T-operator [41]. Even if the interaction is TRI, T-odd correlation term may exist because of the effect of final state interaction (FSI). We must evaluate the FSI effect and subtract it from the observed T-odd correlation term. The measurement of a T-odd correlation term in nuclear β-decay is a good example to see the problem of FSI effects. The T-odd correlation term $D\hat{\mathbf{J}}\cdot(\vec{p}_e \times \vec{p}_\nu)/(E_e E_\nu)$ in $^{19}Ne \rightarrow {}^{19}F + e^+ + \nu$ was measured [42] where $\hat{\mathbf{J}}$, $\vec{p}_e$, $\vec{p}_\nu$, E_e and E_ν are a unit vector parallel to the nuclear spin of ^{19}Ne, momenta of the emitted positron and neutrion, kinetic energies of positron and neutrino, respectively. The obtained result is $D = (4 \pm 8) \times 10^{-4}$, while the contribution of FSI is $\sim 2.6 \times 10^{-4} p_e/(p_e)_{max}$, where $(p_e)_{max}$ is the maximum value of p_e [43]. The experimental sensitivity to T-violation is limited to a few times 10^{-4} by the value of the contribution of the FSI effect. The FSI effect appears in all decay or reaction processes. But it does not exist when the system is static, or the process is elastic scattering where momenta of incoming and outgoing particles are the same. In such cases, there is no contribution of FSI effect to a T-odd correlation term, and a non-zero value of T-odd correlation term is equivalent to the existence of T-violation. This feature is suitable for the measurement of small T-violating effects.

A non-zero value of an electric-dipole-moment (EDM) of a fermion violates TRI and it is an observable in a static system. The measurement of neutron EDM (d_n) has provided the most reliable upper limit for TRI. Recent improvement of techniques to storage ultra-cold-neutrons in a bottle has greatly reduced the systematic error due to the Larmor precession about an effective magnetic field

which is induced by Lorentz transformation from the electric field applied to detect the EDM. The upper limits $d_n = (0.6 \pm 0.6) \times 10^{-25}\mathrm{e}\cdot cm$ and $d_n = -(1.4 \pm 0.6) \times 10^{-25}\mathrm{e}\cdot cm$ have been obtained at ILL [44] and Leningrad [45], respectively[2]. These results give an upper limit of the order of 10^{-3} [39] for the strength of T-odd interaction relative to that of T-even interaction.

In neutron transmission experiments, kinds and momenta of incoming and outgoing particles are the same, and no FSI effect is contained in T-odd correlation terms. In most of these cases, we can test TRI only in the strong interaction. But a sizable contribution of the weak interaction is contained in the vicinity of p-wave resonances where large PNC effects are observed. Therefore, if we observe T-odd correlation terms in the vicinity of such p-wave resonances, we can study T-violating effect in the weak interaction free from FSI.

It is very important to study the reaction mechanism of capture reaction where large PNC effects are observed, in order to find the most suitable nucleus and the most efficient method for TRI experiment.

There have been two types of experiments for the measurement of longitudinal asymmetry. One of them is the measurement of helicity dependence of neutron beam attenuation. This method is referred to as neutron transmission method hereafter. The total cross section is measured in the neutron transmission method. The other one is the measurement of helicity dependence of the cross section of neutron radiative capture reaction. Capture γ-rays are measured in this method which is referred to as γ-ray detection method. The γ-ray detection method is more efficient than the neutron transmission method for the measurement of longitudinal asymmetry, since the γ-ray detection method is insensitive to a very large potential scattering cross section in which no large PNC effect has been observed.

The γ-ray detection method has further merit. In the neutron transmission method, the capture cross section consists of only two terms. Those are a helicity independent term and a helicity dependent term $(\boldsymbol{\sigma}_n \cdot \hat{\boldsymbol{k}}_n)$ where $\boldsymbol{\sigma}_n$ is incident neutron spin and $\hat{\boldsymbol{k}}_n$ is the unit vector parallel to neutron momentum. In the γ-ray detection method, the capture cross section consists of more terms which depend on the neutron helicity and the polar angle of the γ-ray momentum with respect to the beam axis (θ). The θ dependence arises from the interference in the exit channel of the compound state. The measurement of the θ dependence enables us to study details of reaction mechanism since each term contains information of different reaction mechanisms.

The longitudinal asymmetry of the p-wave resonance for a ^{139}La target ($E_n = 0.734eV$) had been measured at Dubna [23, 24] and KEK [25], where E_n is the energy of incident neutrons. The value $A_L = (7.3 \pm 0.5)\%$ was obtained by neutron transmission method, while $A_L = (9.5 \pm 0.3)\%$ was obtained at KEK by

[2]The latter one is interpreted as an upper limit of $|d_n| < 2.6 \times 10^{-25}\mathrm{e}\cdot cm$ at a 95% confidence level.

γ-ray detection method [3]. In general, the longitudinal asymmetry obtained in γ-ray detection method is not equivalent to that obtained in neutron transmission method because of θ dependent terms. The γ-ray detection method is equivalent to neutron transmission method only when the γ-rays are detected in whole solid angle. Vanhoy et al. [46] suggested a possibility that the inconsistency between two values are due to θ dependent terms, since γ-rays were detected for incomplete solid angle around $\theta = 90°$. The measurement of θ dependences is very important to study the origin of the discrepancy.

In this work, we have carried out a precise measurement of helicity dependence and θ dependence in p-wave resonance cross sections with improved equipment to investigate the PNC effect in n-A interactions. Longitudinal asymmetries have been measured in p-wave resonances for ^{81}Br, ^{93}Nb, ^{108}Pd, ^{111}Cd, ^{124}Sn and ^{139}La targets. We have measured the number of γ-rays above $1\,MeV$ without identifying individual γ-ray transitions.

We have also carried out the following measurements to study the contribution of an interference term in the exit channel of a compound state. (1) The θ dependence has been studied for ^{81}Br and ^{139}La target nuclei to study the exit-channel interference effects in the measurement with $1\,MeV$ γ-ray energy threshold levels. (2) The longitudinal asymmetry for ^{139}La target has been measured as a function of energy threshold levels for γ-ray detection. (3) The parity violating angular distribution of γ-rays with respect to the spin direction of incident neutrons which corresponds to the $(\boldsymbol{\sigma}_n \cdot \hat{\boldsymbol{k}}_\gamma)$ term has been measured for ^{139}La target, where $\hat{\boldsymbol{k}}_\gamma$ is the unit vector parallel to γ-ray momentum.

The dependence of longitudinal asymmetry on incident neutron energy (E_n) has been studied for a ^{139}La target. A cold target was used to obtain a better energy resolution by reducing a Doppler broadening.

The formalism of θ dependence in $(\vec{n}, \gamma)$ reaction is given in section 2. The experimental procedures and characteristics of detectors are described in section 3 and section 4. The method of data analysis and experimental results are discussed in section 5. Theoretical interpretation based on parity mixing in the first order perturbation is discussed in section 6 and section 7. In section 8, we give an overview of further study of PNC effects. We also point out a feasibility of a TRI experment to measure the P-odd T-odd triple vector correlation term $(\boldsymbol{\sigma}_n \cdot (\hat{\mathbf{I}} \times \hat{\boldsymbol{k}}_n))$ in neutron transmission method, where $\hat{\mathbf{I}}$ is the unit vector parallel to the target nuclear spin [47].

2 Formalism of $(\vec{n}, \gamma)$ Reaction Cross Section

In this section, we describe the formalism of a $(\vec{n}, \gamma)$ reaction cross section.

[3] Recoently, Los Alamos group [28] obtained the value of the A_L for the same resonance which confirms the value obtained at KEK.

A number of compound resonances are observed in the capture reaction. In epithermal neutron capture reactions, the s-wave component of incident neutron is dominant, and p-wave component is very small. Higher components are negligible due to the centrifugal potential barrier. Therefore, we assume that all processes in this energy region can be described by the contributions of s- and p-wave components. If only s- and p-wave components exist, the differential cross section of radiative capture reaction induced by polarized neutrons ($\sigma_{n\gamma}(\boldsymbol{\sigma}_n, \hat{\boldsymbol{k}}_n, \boldsymbol{\sigma}_\gamma, \hat{\boldsymbol{k}}_\gamma)$) can be written as

$$\begin{aligned}\sigma_{n\gamma}(\boldsymbol{\sigma}_n, \hat{\boldsymbol{k}}_n, \boldsymbol{\sigma}_\gamma, \hat{\boldsymbol{k}}_\gamma) = \frac{1}{2}\Bigg(& a_0 + a_1 \hat{\boldsymbol{k}}_n \cdot \hat{\boldsymbol{k}}_\gamma + a_2 \boldsymbol{\sigma}_n \cdot (\hat{\boldsymbol{k}}_n \times \hat{\boldsymbol{k}}_\gamma) + a_3 \left((\hat{\boldsymbol{k}}_n \cdot \hat{\boldsymbol{k}}_\gamma)^2 - \frac{1}{3} \right) \\ & + a_4 (\hat{\boldsymbol{k}}_n \cdot \hat{\boldsymbol{k}}_\gamma)(\boldsymbol{\sigma}_n \cdot (\hat{\boldsymbol{k}}_n \times \hat{\boldsymbol{k}}_\gamma)) + a_5 (\boldsymbol{\sigma}_\gamma \cdot \hat{\boldsymbol{k}}_\gamma)(\boldsymbol{\sigma}_n \cdot \hat{\boldsymbol{k}}_\gamma) \\ & + a_6 (\boldsymbol{\sigma}_\gamma \cdot \hat{\boldsymbol{k}}_\gamma)(\boldsymbol{\sigma}_n \cdot \hat{\boldsymbol{k}}_n) \\ & + a_7 (\boldsymbol{\sigma}_\gamma \cdot \hat{\boldsymbol{k}}_\gamma) \left((\boldsymbol{\sigma}_n \cdot \hat{\boldsymbol{k}}_\gamma)(\hat{\boldsymbol{k}}_\gamma \cdot \hat{\boldsymbol{k}}_n) - \frac{1}{3} \boldsymbol{\sigma}_n \cdot \hat{\boldsymbol{k}}_n \right) \\ & + a_8 (\boldsymbol{\sigma}_\gamma \cdot \hat{\boldsymbol{k}}_\gamma) \left((\boldsymbol{\sigma}_n \cdot \hat{\boldsymbol{k}}_n)(\hat{\boldsymbol{k}}_n \cdot \hat{\boldsymbol{k}}_\gamma) - \frac{1}{3} \boldsymbol{\sigma}_n \cdot \hat{\boldsymbol{k}}_\gamma \right) \\ & + a_9 \boldsymbol{\sigma}_n \cdot \hat{\boldsymbol{k}}_\gamma + a_{10} \boldsymbol{\sigma}_n \cdot \hat{\boldsymbol{k}}_n \\ & + a_{11} \left((\boldsymbol{\sigma}_n \cdot \hat{\boldsymbol{k}}_\gamma)(\hat{\boldsymbol{k}}_\gamma \cdot \hat{\boldsymbol{k}}_n) - \frac{1}{3} \boldsymbol{\sigma}_n \cdot \hat{\boldsymbol{k}}_n \right) \\ & + a_{12} \left((\boldsymbol{\sigma}_n \cdot \hat{\boldsymbol{k}}_n)(\hat{\boldsymbol{k}}_n \cdot \hat{\boldsymbol{k}}_\gamma) - \frac{1}{3} \boldsymbol{\sigma}_n \cdot \hat{\boldsymbol{k}}_\gamma \right) \\ & + a_{13} \boldsymbol{\sigma}_\gamma \cdot \hat{\boldsymbol{k}}_\gamma + a_{14} (\boldsymbol{\sigma}_\gamma \cdot \hat{\boldsymbol{k}}_\gamma)(\hat{\boldsymbol{k}}_n \cdot \hat{\boldsymbol{k}}_\gamma) + a_{15} (\boldsymbol{\sigma}_\gamma \cdot \hat{\boldsymbol{k}}_\gamma) \boldsymbol{\sigma}_n \cdot (\hat{\boldsymbol{k}}_n \cdot \hat{\boldsymbol{k}}_\gamma) \\ & + a_{16} (\boldsymbol{\sigma}_\gamma \cdot \hat{\boldsymbol{k}}_\gamma) \left((\hat{\boldsymbol{k}}_n \cdot \boldsymbol{k}_\gamma)^2 - \frac{1}{3} \right) \\ & + a_{17} (\boldsymbol{\sigma}_\gamma \cdot \hat{\boldsymbol{k}}_\gamma)(\hat{\boldsymbol{k}}_n \cdot \hat{\boldsymbol{k}}_\gamma)(\boldsymbol{\sigma}_n \cdot (\boldsymbol{k}_n \times \hat{\boldsymbol{k}}_\gamma)) \Bigg), \end{aligned} \tag{7}$$

where $\boldsymbol{\sigma}_n$ and $\boldsymbol{\sigma}_\gamma$ are spins of neutron and γ-ray, $\hat{\boldsymbol{k}}_n$ and $\hat{\boldsymbol{k}}_\gamma$ are unit vectors parallel to momenta of neutron and γ-ray, respectively [48]. When the circular polarization of γ-ray $(\boldsymbol{\sigma}_\gamma \cdot \hat{\boldsymbol{k}}_\gamma)$ is not observed and the incident neutrons are longitudinally polarized, capture cross sections for incident positive- and negative-helicity neutrons, represented by $\sigma^+_{n\gamma}(\theta)$ and $\sigma^-_{n\gamma}(\theta)$, can be written as

$$\begin{aligned}\sigma^{\pm}_{n\gamma}(\theta) = \frac{1}{2}\Bigg(& a_0 + a_1 \cos\theta + a_3 (\cos^2\theta - \frac{1}{3}) \\ & \pm \left(a_{10} + (a_9 + \frac{2}{3} a_{12}) \cos\theta + a_{11} (\cos^2\theta - \frac{1}{3}) \right) \Bigg), \end{aligned} \tag{8}$$

where θ is the polar angle of γ-ray momentum. The integrated capture cross section for incident unpolarized neutrons ($\sigma_{n\gamma}$) is

$$\sigma_{n\gamma} = \frac{1}{2}\int (\sigma^{+}_{n\gamma}(\theta) + \sigma^{-}_{n\gamma}(\theta))\, d\Omega = 2\pi a_0. \tag{9}$$

When we look at vicinity of a p-wave resonance, we can observe a component which changes slowly with incident neutron energy (E_n) in addition to the component of the p-wave resonance. The resonance part of the capture cross section is represented by σ_r hereafter. We parametrize the angular dependence of the resonance component of capture cross section as

$$\begin{aligned}\sigma^{\pm}_r(\theta) = \sigma_r \times \Bigg(1 + \alpha_{01}\cos\theta + \alpha_{02}\left(\cos^2\theta - \frac{1}{3}\right) \\ \pm \left(A_L + \alpha_{L1}\cos\theta + \alpha_{L2}\left(\cos^2\theta - \frac{1}{3}\right)\right)\Bigg).\end{aligned} \tag{10}$$

The a_0 term in Eq. 7 consists of s-wave and p-wave components represented by a_{0s} and a_{0p}, respectively ($a_0 = a_{0s} + a_{0p}$). We assume that an s-wave and a p-wave resonances exist in the region of our interest and the continuum component depends on neither θ nor incident neutron helicity. Then, the cross section of the continuum component equals to $2\pi a_{0s}$. If we write $A_i = a_i/a_{0p}$, we obtain

$$a_{01} = A_1, \quad \alpha_{02} = A_3, \quad A_L = A_{10}, \quad \alpha_{L1} = A_9 + \frac{2}{3}A_{12}, \quad \alpha_{L2} = A_{11}. \tag{11}$$

The resonance cross section obtained in neutron transmission experiments corresponds to

$$\sigma^{\pm}_r = \int \sigma^{\pm}_r(\theta)\, d\Omega \propto 1 \pm A_L. \tag{12}$$

Therefore the longitudinal asymmetry measured in transmission method is equivalent to A_L defined in Eq. 10.

The helicity dependent asymmetry of the resonance component of capture γ-rays represented by $a_{L,\gamma}(\theta)$ is given as

$$a_{L,\gamma}(\theta) = \frac{\sigma^{+}_r(\theta) - \sigma^{-}_r(\theta)}{\sigma^{+}_r(\theta) + \sigma^{-}_r(\theta)} = \frac{A_L + \alpha_{L1}\cos\theta + \alpha_{L2}\left(\cos^2\theta - \frac{1}{3}\right)}{1 + \alpha_{01}\cos\theta + \alpha_{02}\left(\cos^2\theta - \frac{1}{3}\right)}. \tag{13}$$

There are three ways to determine the value of longitudinal asymmetry A_L in γ-ray detection method. The first one is to detect capture γ-rays for whole solid angle. The second one is to determine all parameters in Eq. 13. We can determine all parameters by measuring the helicity dependent asymmetries $a_{L,\gamma}(\theta)$ and the angular distribution of capture γ-ray intensity induced by incident unpolarized

neutrons. The last one is to measure the helicity dependent asymmetries $a_{L,\gamma}(\theta)$ at two θ's which satisfy $\cos^2\theta - 1/3 = 0$. Substituting $\theta = \theta_0$, $\pi - \theta_0$ into Eq. 10 where θ_0 is one of the solutions of $\cos^2\theta - 1/3 = 0$, we obtain

$$\begin{aligned} \sigma_r^{\pm}(\theta_0) &= \sigma_r \times (1 + \alpha_{01}\cos\theta_0 \pm (A_L + \alpha_{L1}\cos\theta_0)), \\ \sigma_r^{\pm}(\pi - \theta_0) &= \sigma_r \times (1 - \alpha_{01}\cos\theta_0 \pm (A_L - \alpha_{L1}\cos\theta_0)). \end{aligned} \tag{14}$$

The A_L is obtained as

$$A_L = \frac{\langle\sigma_r^+\rangle - \langle\sigma_r^-\rangle}{\langle\sigma_r^+\rangle + \langle\sigma_r^-\rangle}, \tag{15}$$

where $\langle\sigma_r^{\pm}\rangle = (\sigma_r^{\pm}(\theta_0) + \sigma_r^{\pm}(\pi - \theta_0))/2$.

We define forward-backward asymmetry represented by a_γ as

$$\sigma_r^{\pm}(\theta) \propto (1 \pm A_L)(1 \pm a_\gamma \cos\theta). \tag{16}$$

The a_γ is a parity violating angular distributin of capture γ-rays with respect to the spin of incident neutrons. The a_γ is approximately equivalent to α_{L1} if $a_\gamma A_L \ll 1$ and $\theta \simeq \theta_0$ hold. The α_{L1} is approximately equal to A_9 since the A_{12} is negligibly small compared with A_9 (Appendix A). Consequently, the a_γ is approximately equal to A_9. The a_γ changes its sign at the resonance energy, since the a_9 has a dispersive E_n dependence in the vicinity of the p-wave resonance (see Eq. 47) as shown in

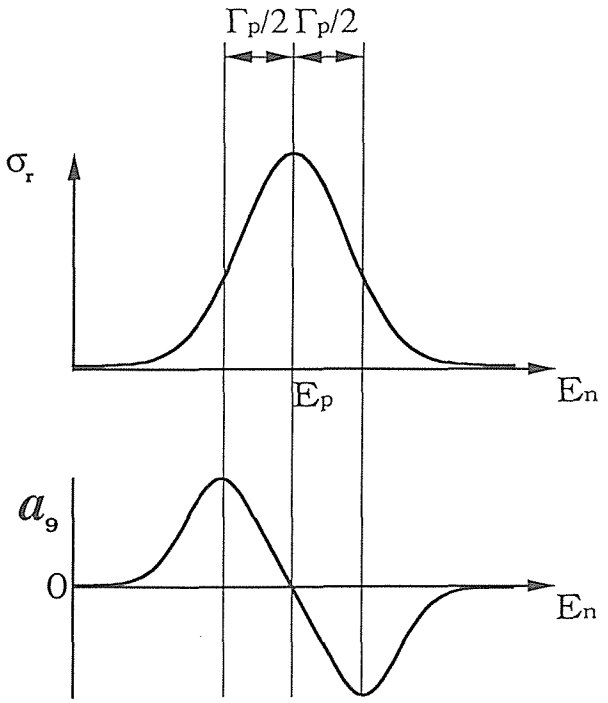

Fig. 1. The E_n dependence of a_9 in the vicinity of the p-wave resonance is shown. The E_p and Γ_p are the resonance energy and the resonance width of the resonance, respectively.

Fig. 1, where E_n is the energy of incident neutrons. The a_γ, thus, must be calculated in left- or right-hand side of the p-wave resonance. We use $a_{\gamma,<}$, $a_{\gamma,>}$ and $a_{\gamma,<>}$ to represent the a_γ calculated in the energy region of $E_p - \Gamma_p \leq E_n \leq E_p$, $E_p \leq E_n \leq E_p + \Gamma_p$ and $E_p - \Gamma \leq E_n \leq E_p + \Gamma_p$, respectively. The E_p and Γ_p are resonance energy and the resonance width of the p-wave resonance, respectively. We write the difference between $a_{\gamma,<}$ and $a_{\gamma,>}$ as

$$\langle a_\gamma \rangle = \frac{a_{\gamma,<} - a_{\gamma,>}}{2}. \tag{17}$$

3 Neutron Beam

The experiment has been carried out at Booster Synchrotron utilization Facility at KEK. The neutron beam was obtained from the spallation neutron source at KEK. A dynamically polarized proton filter was used to obtain the neutron polarization. The obtained neutron polarization was $\sim 70\,\%$ for $1eV$ neutrons. In this section, we describe the spallation neutron source and the neutron polarizer.

3.1 Spallation Neutron Source

A pulsed $500MeV$ proton beam from the booster synchrotron at KEK bombarded a uranium target block for producing neutrons by spallation reactions [49]. The repetition rate of the primary proton beam is $20Hz$. The intensity of the proton beam is $(5 \sim 15) \times 10^{11}$ protons per pulse. Neutrons are moderated in

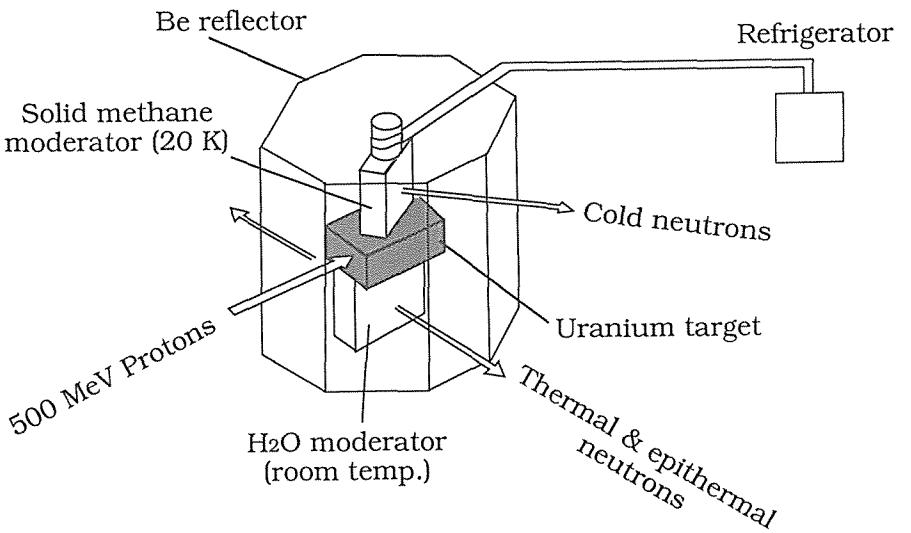

Fig. 2. The neutron source complex at KEK is schematically shown. A uranium target of $7.8\,cm^W \times 5.7\,cm^H \times 3.0\,cm^T$ is sandwiched with two moderators. One is a water cell of $10.0\,cm^W \times 10.0\,cm^H \times 5.0\,cm^T$ (room temperature) which provides thermal neutrons and epithermal neutrons. The other is a solid methane ($20\,K$) which provides cold neutrons. Our beam line is on the level of the former one.

a water cell which is placed under the uranium target (Fig. 2). The uranium target and the moderator are shielded by a $4m$ thick biological shield made of iron and concrete.

The neutron energy was determined by the time-of-flight (TOF) method using a multi-channel-scaler (MCS: CANBERRA-7880 and equivalent CAMAC modules). A sweep of MCS was started by a pulse of the primary proton beam, and detected events were histogramed against the time difference between the starting of the sweep and the occurrence of an event. The time bin width of MCS was set to be $0.25 \sim 1\mu s$ which corresponds to neutron energy resolution of $0.001 \sim 0.004eV$ for $1eV$ neutrons with $6.6m$ flight path. The neutron energy determined by the TOF method contains an error which arises from the distribution of the time when moderated neutrons of an energy leave the moderator. The time width of the distribution for $1eV$ neutrons is $\simeq 1.3\mu s$ in FWHM [50] which corresponds to $0.005eV$ energy spread when $6.6m$ flight path is taken.

The size of neutron beam was defined by a collimator placed upstream a neutron polarizer. A typical neutron intensity versus neutron energy is shown in Fig. 3. The neutron intensity was measured using a ^{10}B loaded liquid scintillator (NE311A) placed at $9.4m$ from the neutron source. The number of neutrons incident to the polarizer was monitored by counting capture γ-rays from an annular indium foil placed at $4.5m$ from the neutron source [51].

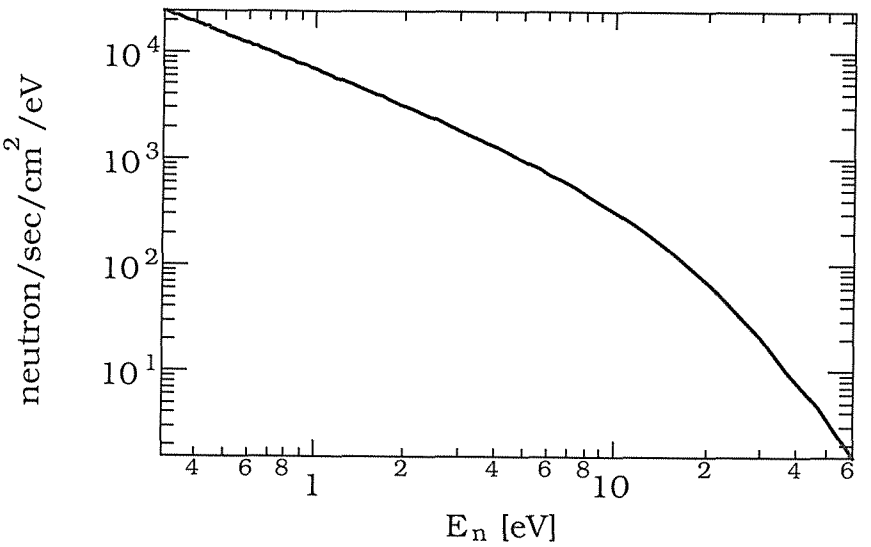

Fig. 3. Neutron intensity at PEN beam line upstream the polarized proton filter versus incident neutron energy. The intensity of the primary proton beam was 7×10^{11} [*proton/pulse*] $\times$ 20 [*pulse/sec*].

3.2 Neutron Polarizer

Incident neutrons were transversely polarized upon transmission through a proton filter which was dynamically polarized in the vertical direction, due to a spin dependence of proton-neutron cross section [52, 53, 54, 55, 56, 57]. The

dynamically polarized proton filter was installed at $5.2m$ from the neutron source. The layout of the polarized proton filter is shown in Fig. 4. Superconducting coils and a ^3He cryostat were installed in the same liquid-helium container. The magnetic flux density at the center of the filter was $2.5T$ with homogeneity of 0.5×10^{-4} in a volume of $3cm$ diameter and $4cm$ height. The coils were designed to be asymmetric with respect to the field direction. The ^3He cryostat was a continuous-flow type and was installed at the center of the liquid helium container. The ^3He gas was pumped out by a Roots pump system (Alcatel RSV2000 + RSV350 + 2060H). The temperature of liquid ^3He was less than $0.5K$. The polarized proton filter was placed in a copper box as shown in Fig. 5. The filter consisted of 5 layers of plates ($3.3 \times 2.4 \times 0.2cm^3$) with spacing of $0.2cm$. This box was cooled by liquid ^3He from outside through heat exchanging copper fins which were attached from inside and outside of the box. The box was filled with ^4He superfluid liquid which worked as a heat exchanger between the box and the filter layers. The neutron beam passed through these plates in their normal direction. Neutron absorption by the ^3He gas in the neutron flight path was negligible since the ^3He gas pressure was less than $0.16Torr$ and the length of the flight path was $4cm$.

Microwave of $70GHz$ was supplied to the filter through the wave guide. The microwave was obtained by using a klystron (OKI-KA704A). The microwave

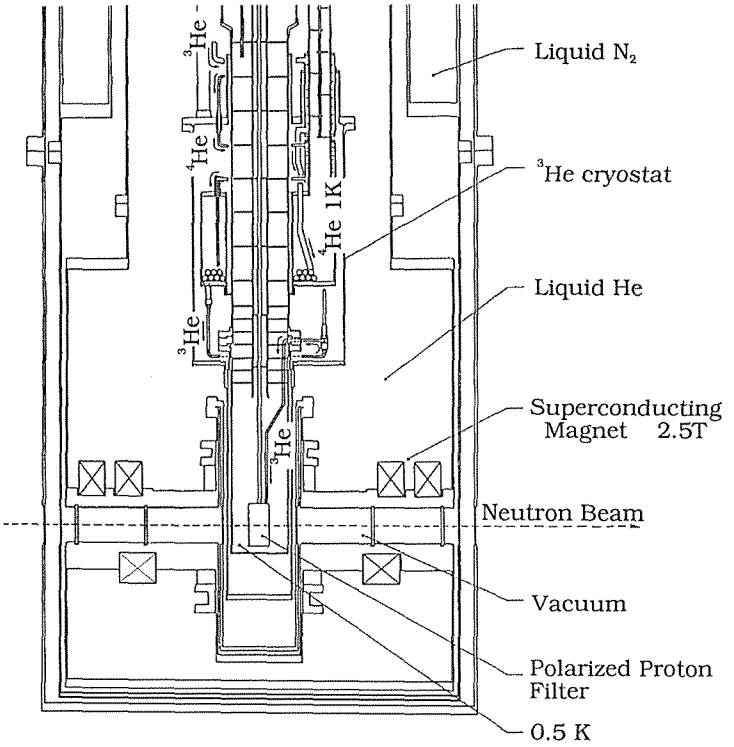

Fig. 4. The arrangement of the dynamically polarized proton filter as a neutron-spin polarizer.

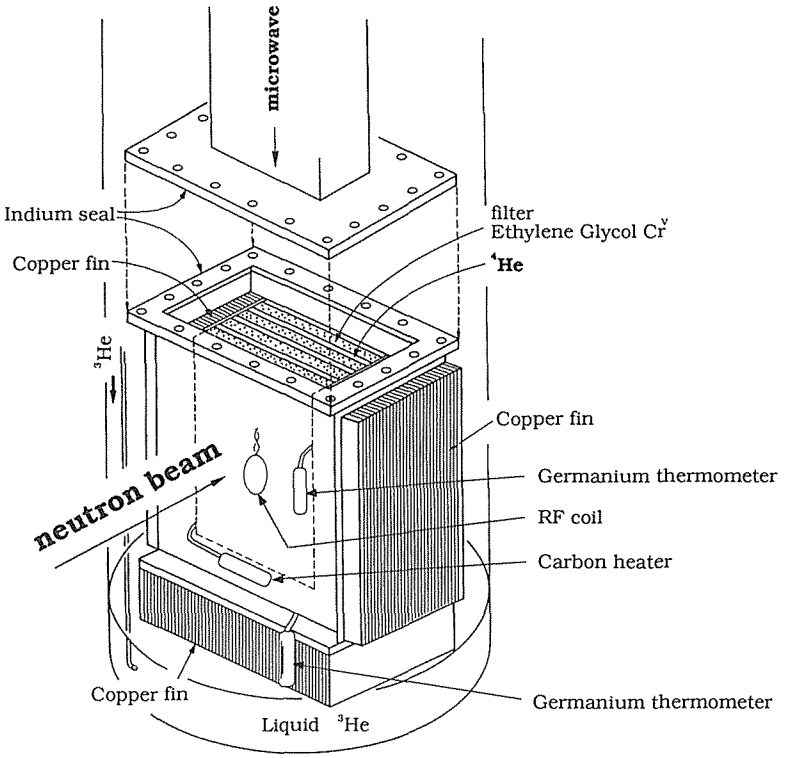

Fig. 5. The configuration of the copper box cavity containing five layers of ethylene glycol (Cr^V). The box is helium tight and filled with liquid ^4He for heat conductor between the ethylene glycol layer and the box. The walls of the box were grooved and formed into fins. The depths of the grooves are from 0.5 to $1\,cm$. The thickness of the fins is around $0.03\,cm$ and the gap between the fins is $0.03\,cm$. The bottom of the box is immersed in a liquid ^3He bath.

power was about $35\,mW$ at the filter.

The filter material was cooked in chemical reaction. The $50\,cm^3$ ethylene-glycol was kept at the temperature of $70°C$. Powder of potassium dichromate ($K_2Cr_2O_7$) of $22\,g$ was added to it, and the mixture was stirred for $12\,min$ at $70°C$. Complexes of Cr^V were produced in the reaction. The Cr^V was used as free radicals for the dynamic polarization. The optimum density of Cr^V was approximately one per 200 hydrogens which corresponds to the electron density of $3 \times 10^{20}\,cm^{-3}$. The proton polarization of about 80 % was obtained at $0.5\,K$. The proton polarization was monitored every minute with an NMR-coil embedded in the filter material. The fluctuation of the polarization was within a few percent for a few weeks.

The neutron transmittance of the polarized proton filter was measured for unpolarized filter and polarized filter using the liquid scintillator to measure neutron polarization. Here we describe a method to measure neutron polarization. The numbers of spin-up and spin-down neutrons after transmission through a polarized proton filter are given as

$$N_n^{\uparrow} = \frac{N_n^I}{2}\exp\left(-\frac{n_p}{2}((1+p_p)\sigma_{pn}^{\uparrow\uparrow} + (1-p_p)\sigma_{pn}^{\uparrow\downarrow}t\right),$$
$$N_n^{\downarrow} = \frac{N_n^I}{2}\exp\left(-\frac{n_p}{2}((1-p_p)\sigma_{pn}^{\uparrow\uparrow} + (1+p_p)\sigma_{pn}^{\uparrow\downarrow})t\right), \tag{18}$$

respectively, where N_n^I is the number of incident neutrons, n_p is the number density of protons, t is the thickness of the filter, p_p is the proton polarization and $\sigma_{pn}^{\uparrow\uparrow}(\sigma_{pn}^{\uparrow\downarrow})$ is the total cross section for parallel (anti-parallel) spins. The neutron polarization p_n is given as

$$p_n = \frac{N_n^{\uparrow} - N_n^{\downarrow}}{N_n^{\uparrow} + N_n^{\downarrow}} = \tanh\left(\frac{n_p}{2}p_p \Delta\sigma_{pn}t\right), \tag{19}$$

where $\Delta\sigma_{pn} = \sigma_{pn}^{\uparrow\uparrow} - \sigma_{pn}^{\uparrow\downarrow}$. The number of neutrons transmitted through polarized filter is

$$N_n^P = N_n^{\uparrow} + N_n^{\downarrow} = N_n^I \exp(-n_p\sigma_{pn}^0 t)\cosh\left(\frac{n_p}{2}p_p\Delta\sigma_{pn}t\right), \tag{20}$$

where $\sigma_{pn}^0 = (\sigma_{pn}^{\uparrow\uparrow} + \sigma_{pn}^{\uparrow\downarrow})/2$. The number of neutrons transmitted through unpolarized filter is

$$N_n^U = N_n^I \exp(-n_p\sigma_{pn}^0 t). \tag{21}$$

The neutron transmittance of polarized filter (T_n^P) relative to that of unpolarized filter (T_n^U) is

$$\frac{T_n^P}{T_n^U} = \frac{N_n^P}{N_n^U} = \cosh\left(\frac{n_p}{2}p_p\Delta\sigma_{pn}t\right). \tag{22}$$

From Eq. 19 and Eq. 22, we obtain

$$p_n = \sqrt{1 - \left(\frac{T_n^U}{T_n^P}\right)^2}. \tag{23}$$

The validity of this formula had been confirmed within the accuracy of 3 % relative to the neutron polarization for $E_n > 0.2eV$ [57, 52] which covers the region of our interest. A typical neutron polarization versus neutron energy is shown in Fig. 6.

The neutron spins were rotated from transverse to longitudinal direction following an adiabatic passage which was the superposed field of fringing field of superconducting coils and longitudinal field of the $150G$ solenoid placed downstream the polarizer. The helicity of incident neutrons was reversed every 2.5 or $4sec$ by changing the magnetic field direction of the solenoid. The depolarization in the adiabatic passage is calculated to be within 1 % relative to the original polarization for neutrons whose energies are less than $100eV$. The calculation has been carried out by a numerical simulation using the measured value of magnetic field along the neutron flight path.

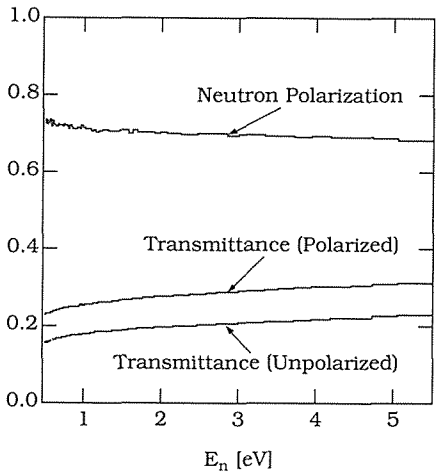

Fig. 6. Neutron polarization is plotted with transmittance of polarized and unpolarized filters.

4 Experimental Procedures

In this section, the experimental procedures are described. Three kinds of measurement have been carried out in the experiment. One is the measurement of helicity dependence of capture γ-ray intensities, that is, longitudinal asymmetry A_L (see Eq. 11) in several p-wave resonances for several target nuclei. It has been carried out using a BaF_2 γ-ray counter which covers a large solid angle. Angular dependences of $a_{L,\gamma}(\theta)$ (Eq. 13) have been also studied in the same measurement. Another one is the measurement of angular distributions of capture γ-rays induced by incident unpolarized neutrons of p-wave resonances for ^{139}La and ^{81}Br target nuclei. This measurement is necessary to determine all parameters in Eq. 13. The other one is the measurement of longitudinal asymmetry of the p-wave resonance for ^{139}La target nucleus with better γ-ray energy resolution using a γ-ray counter with bismuth germanate ($Bi_4Ge_3O_{12}$: BGO) crystals. A few γ-ray transitions have been selected with higher γ-ray energy threshold. The forward-backward asymmetry (Eq. 17) has been also studied in the same measurement.

4.1 Measurement of Longitudinal Asymmetry

The longitudinal asymmetries have been measured for ^{81}Br, ^{93}Nb, ^{108}Pd, ^{111}Cd, ^{124}Sn and ^{139}La target nuclei using a BaF_2 scintillation counter which covers a large solid angle. The setup of the experiment is shown in Fig. 7 and the configuration of the γ-ray counter is shown in Fig. 8 [51].

At $6.6m$ from the neutron source, a target disk of $2.5cm$ in diameter was placed in a $50G$ solenoid which held the neutron spin direction. Used target materials are listed in Table 3. All the elements in the targets had natural abundances. The size of longitudinally polarized neutron beam was defined to $1.8cm$ in diameter by B_4C collimators placed in the $50G$ solenoid. A cylinder made of sintered B_4C was

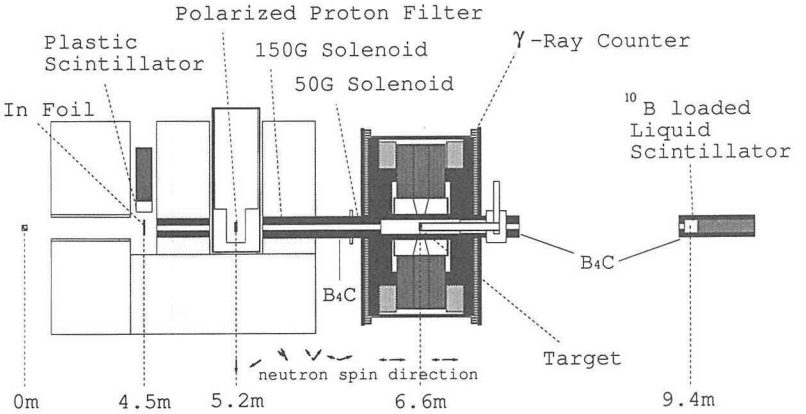

Fig. 7. The experimental setup of PEN beam line is schematically shown with a γ-ray counter for the measurement of A_L and $a_{L,\gamma}(\theta)$ (see Fig. 8 for details of the γ-ray counter).

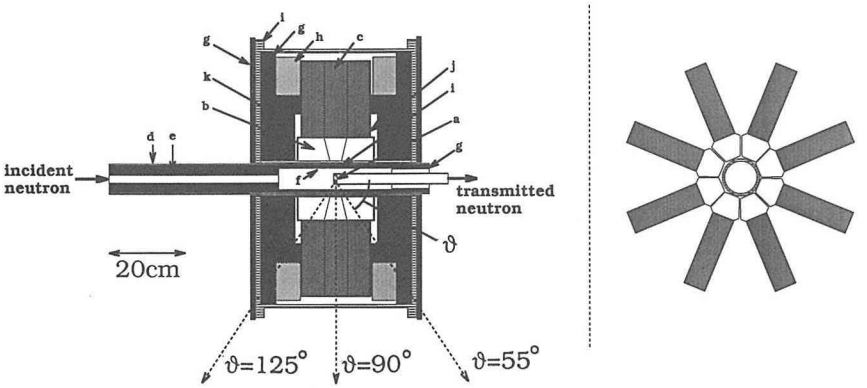

Fig. 8. The BaF_2 γ-ray counter for the measurement of the A_L and the $a_{L,\gamma}(\theta)$. (a) Target, (b) BaF_2 crystals, (c) UV sensitive photomultipliers, (d) $50G$ solenoid, (e) B_4C (neutron absorber), (f), sintered B_4C (neutron absorber), (g) B_4C (neutron absorber), (h) boric acid resin (neutron absorber), (i) iron (magnetic shield), (j) μ metal (magnetic shield), (k) lead (γ-ray absorber). A cross section of counter configuration seen from down stream on the beam line is shown in the right hand side. The BaF_2 crystals are arranged to detect γ-rays at $\theta = 55°$, $90°$ and $125°$. The BaF_2 crystals cover 85 % of 4π steradians in total.

Table 3. List of target materials. The areal densities of relevant isotopes are shown.

nucleus	material	thickness [cm]	areal density $[\times 10^{22} nuclei/cm^2]$	target temperature
^{81}Br	CBr_4	3.0	2.9	room temp.
	CBr_4	5.0	5.2	room temp.
^{93}Nb	metal	2.5	13.9	room temp.
^{108}Pd	metal	0.7	1.8	room temp.
^{111}Cd	metal	1.15	0.68	room temp.
^{124}Sn	metal	3.0	0.17	room temp.
^{139}La	metal	1.0	2.7	$35K$
	metal	0.3	0.8	$9K$

inserted inside the solenoid to absorb scattered neutrons from the target so that the scattered neutron does not produce capture γ-rays outside the target.

The BaF_2 crystals were used as γ-ray detectors. The BaF_2 crystal has various attractive properties [58]. Its radiation length is short ($X_0 = 2.1 cm$) and its density is high ($\rho = 4.88 g/cm^3$). The light output of BaF_2 amounts to $\sim 1/5$ of that of $NaI(Tl)$. The BaF_2 crystal has two light emission peaks at 220 and $310 nm$ in wave length. The decay constants for the two components are 0.6 and $620 ns$. Hamamatsu R329QTE photomultipliers with $CsTe$ photocathode were used to detect only the fast component ($220 nm$) of the scintillation light with good timing characteristics. A quartz plate was used as a window for the R329QTE so as to transmit the fast component of the light in the ultra violet region. The energy resolution was about 20% for $1 MeV$ γ-rays. The energy threshold level for γ-ray detection was set to $\sim 1 MeV$.

Three γ-ray counters were arranged to detect γ-rays at $\bar{\theta} = 55.5$, 90° and 124.5°, where $\bar{\theta}$ is the averaged value of θ weighted by the absorption probability of γ-rays in the BaF_2 crystals. Angular acceptances were ± 13°, ± 9° and ± 13° in standard deviations. The angle of $\theta = 30° \sim 150°$ (85% of whole solid angle) was covered.

The thickness of the crystal was more than $6 cm$. The scintillators and photomultipliers were put in magnetic shields made of μ-metal. They were covered by $5 cm$ thick lead which reduced background γ-rays. Boric acid resin and B_4C which absorbed background neutrons covered the surface of the lead. The counter box was made of iron which is another magnetic shield. The $2 cm$ thick B_4C walls covered the surface of the counter box to absorb neutrons coming from the neutron source and other beam lines.

The thermal motion of target nuclei causes a Doppler broadening of widths of neutron capture resonances and affects the neutron energy resolution. The width of Doppler broadening of the p-wave resonance for ^{139}La ($E_n = 0.734 eV$) is estimated to be $0.023 eV$ at room temperature by an ideal gas model, while the resonance width is $0.045 eV$. We cooled the lanthanum target down to $29 \sim 40 K$ using a helium refrigerator, and to $9 K$ using a liquid helium cryostat, to reduce the Doppler broadening of the resonance. The Doppler broadening is estimated for the cold targets to be $0.008 eV$ at $35 K$ and $0.004 eV$ at $9 K$, by assuming ideal gas model. Other target materials were put at room temperature since the Doppler broadening is negligible compared with the width of their resonances.

4.2 Measurement of the Angular Distribution

The angular distribution of capture γ-rays induced by unpolarized neutrons have been measured for ^{81}Br and ^{139}La target nuclei with a BGO scintillation counter. The configuration of the γ-ray counter is shown in Fig. 9.

The lanthanum target was a metal column of $2.5 cm$ in diameter and $3.0 cm$ in height. Carbon tetrabromide of the same size was used as the bromine target. All the elements in the targets had natural abundance. The targets were used at room temperature. The size of incident neutron beam was $1.8 cm$ in diameter.

A BGO crystal of $5 cm\phi \times 5 cm$ was used to detect γ-rays from the target with

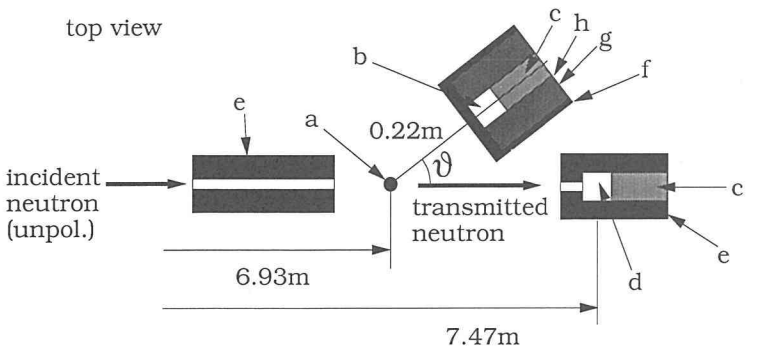

Fig. 9. The schematic view of experimental arrangement of the measurement of angular distribution of capture γ-rays induced by incident unpolarized neutrons. (a) Target, (b) *BGO* crystal, (c) photomultiplier, (d) ^{10}B loaded liquid scintillator, (e, f) B_4C (neutron absorber), (g) lead, (h) iron (magnetic shield).

high detection efficiency. Its radiation length is very short ($X_0 = 1.1\,cm$) and its density is very high ($\rho = 7.1\,g/cm^3$). The detection efficiency is more important than the timing characteristics since the solid angle covered by the crystal is small and the γ-ray counting rate is low. The BGO crystal has a light emission peak at $480\,nm$ in wave length. The scintillation light was detected by a Hamamatsu R1161 photomultiplier. The energy threshold level was set to $\sim 1\,MeV$ for the γ-ray detection. The scintillator and photomultiplier were put in magnetic shields made of iron. They were covered by $5cm$ lead which reduces background γ-rays. Background neutrons were absorbed by the B_4C which covered the surface of the lead. The thickness of B_4C was more than $2\,cm$.

The angular distribution of capture γ-ray intensity was measured at $\theta = 35°$, 50°, 70°, 90°, 110°, 130° and 145°. Angular acceptance of the BGO crystal was $\pm 4°$ in standard deviation. The angular distribution has been measured also for an s-wave resonance of ^{107}Ag target using a $50\,\mu m$ thick silver foil. The γ-ray angular distribution of the s-wave resonance must be uniform since the total angular momentum of the resonance is zero. We checked the detection system using the obtained angular distribution of γ-rays which came from the s-wave resonance.

4.3 Measurement of E_γ Dependence of Longitudinal Asymmetry

The longitudinal asymmetry of the p-wave resonance for ^{139}La target nuclei has been measured with better γ-ray energy resolution and better detection efficiency using BGO crystals.

The experimental setup is schematically shown in Fig. 10. Longitudinally polarized neutron beam defined to a circle of $2.0\,cm$ in diameter by collimators in a solenoid ($50\,G$) bombarded the target disk which was placed at $6.75\,m$ from the neutron source. The target was put at room temperature.

Twelve BGO crystals were used as γ-ray detectors. Scintillation lights were detected by Hamamatsu R1161 photomultipliers. The crystals and photomultipliers were covered by magnetic shields made of μ-metal and put in two iron boxes which

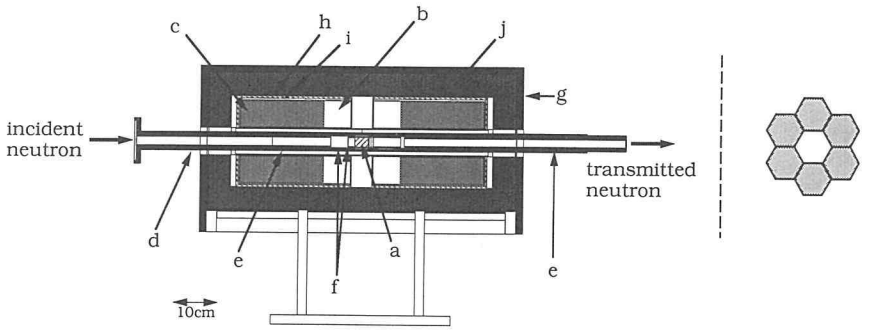

Fig. 10. The BGO γ-ray counter for the measurement of the A_L with different energy threshold levels for γ-ray detection. (a) Target, (b) *BGO* crystals, (c) photomultipliers, (d) $50G$ solenoid, (e) B_4C (neutron absorber), (f) sintered B_4C (neutron absorber), (g) B_4C (neutron absorber), (h) iron (magnetic shield), (i) μ metal (magnetic shield), (j) lead (γ-ray absorber). A cross section of counter configuration seen from downstream on the beam line is shown in the right hand side.

were also magnetic shields. Two iron boxes were covered with $5cm$ lead walls to reduce background γ-rays. The $2cm$ thick B_4C walls covered outside the lead walls to absorb background neutrons. Two sets of BGO detectors were put symmetrically about $\theta = 90°$ so as to obtain the A_L following Eq. 15. Two detector sets covered the angle of $\theta = 20° \sim 70°$ and $\theta = 110° \sim 160°$. The "sensitivity" for the term of $\cos^2\theta - 1/3$ was evaluated as

$$\frac{\int_{\Omega_D} e^{-\ell(\Omega)/\lambda}\left(\cos^2\theta - \frac{1}{3}\right)d\Omega}{\int_{\Omega_D} e^{-\ell(\Omega)/\lambda}\,d\Omega}. \tag{24}$$

The Ω_D is the solid angle covered by scintillators. The $\ell(\Omega)$ is the length of BGO crystal for the direction of Ω. The λ is the mean free path of γ-rays in BGO crystal. The sensitivity depends on γ-ray energy since the λ depends on γ-ray energy. The value of (24) was calculated to be less than 0.04 by averaging in the region of γ-ray energy of $1 \sim 5MeV$.

A typical pulse height spectrum for γ-rays from $^{12}C^*(4.43MeV)$ of an Am/Be radioactive source obtained using this counter is shown in Fig. 11. The energy resolution for 4.43-MeV γ-rays was 13 %.

The pulse height spectrum for γ-rays from $La(n, \gamma)$ ($E_n = 0.46 \sim 1.4eV$) obtained using the same counter is shown in Fig. 12. Bumps are observed around 4.3 and $5MeV$. The labels in the figure indicate the energy where single γ-ray transitions are expected. The expected single γ-ray transitions are listed in Table 4 [59, 60]. The energy threshold levels for γ-ray detection $E_{\gamma,thres}$ were set to $E_{\gamma,thres} = 1.1 \pm 0.1$, 3.2 ± 0.2, 4.2 ± 0.2 and 4.8 ± 0.3 [MeV] [4]. The error of $E_{\gamma,thres}$ is the deviation of photomultiplier gain adjustment among twelve photomultipliers.

[4]The Q-value of $^{139}La + n \rightarrow {}^{140}La$ is $5.2MeV$.

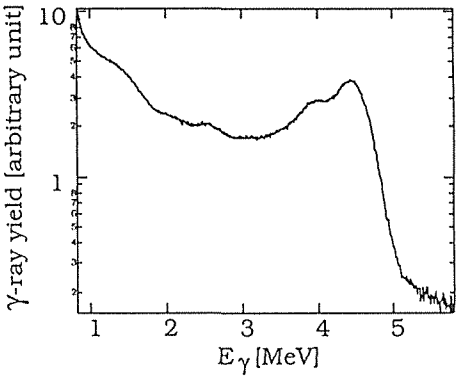

Fig. 11. A typical pulse height spectrum for γ-rays from $^{12}C^*$ (4.43 MeV) of Am/Be radioactive source obtained with the the BGO counter. The horizontal axis is scaled by the pulse height of fully absorbed γ-rays. The energy resolution was 13% in FWHM for 4.43 MeV γ-rays.

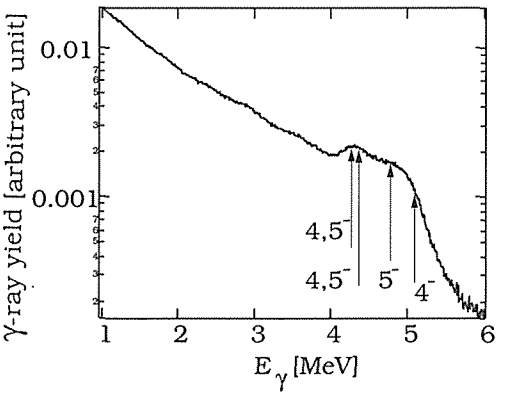

Fig. 12. Typical pulse height spectrum for γ-rays from $La(n, \gamma)$ ($E_n = 0.46 \sim 1.4 eV$) obtained with the BGO counter. The horizontal axis is scaled by the pulse height of fully absorbed γ-rays. The labels show the spin/parity of the final states of expected single γ-ray transitions.

Table 4. The list of spins and parities of final states of relatively intense γ-ray transitions of $^{139}La(n, \gamma)^{140}La$ reported in [59, 60]. The spin and parity of the ground state of ^{140}La is $J^\pi = 3^-$.

E_γ [MeV]	spin/parity of final state
5.101 ± 0.005	4^-
4.845 ± 0.005	5^-
4.416 ± 0.005	$4, 5^-$
4.390 ± 0.005	$4, 5^-$

5 Data Analysis and Results

In this section, we describe the method of the data analysis and the experimental results. In the first subsection, we discuss the data analysis and the experimental results of the measurement of longitudinal asymmetries (A_L in Eq. 11) in several p-wave resonances for several target nuclei using the BaF_2 counter which covers a large solid angle. Angular dependence of helicity dependent asymmetry ($a_{L,\gamma}(\theta)$ in Eq. 13) is also discussed in the same subsection. In the second subsection, we discuss the data analysis and the experimental results of the measurement of angular distributions of γ-rays induced by incident unpolarized neutrons in p-wave resonances for ^{139}La and ^{81}Br target nuclei. The determination of all parameters in Eq. 13 is described in the same subsection. In the last subsection, we discuss the

dependence of longitudinal asymmetry for ^{139}La on energy threshold level for γ-ray detection with better γ-ray energy resolution using the BGO counter. The analysis of forward-backward asymmetry (Eq. 17) is also discussed in the same subsection.

5.1 Longitudinal Asymmetry

The capture γ-ray yields versus inverse velocity of incident neutrons are shown in Fig. 13 for lanthanum, carbon tetrabromide, cadmium, tin, niobium and palladium targets. Background γ-rays are subtracted in the figure. The continuum components obey the $1/v_n$ rule except the case of cadmium target, where v_n is the velocity of incident neutrons. In the case of cadmium target, the continuum component has a nonlinear $1/v_n$ dependence because a large s-wave resonance of ^{113}Cd exists at $E_n = 0.178eV$ close to the plotted region. We extracted the resonance components by subtracting the continuum components. The continuum components were evaluated by least square fitting with a linear function of $1/v_n$ except the case of cadmium target. We used the 3rd order polynomial of $1/v_n$ for the case of cadmium target since it is the lowest order polynomial to reproduce the shape of the continuum component.

The helicity dependent asymmetries of capture γ-ray yields versus incident neutron energy are shown in Fig. 14. They deviate from zero systematically at p-wave resonances for $^{139}La(E_n = 0.734eV)$, $^{81}Br(E_n = 0.88eV)$ and $^{111}Cd(E_n = 4.53eV)$, while no significant deviation has been found at p-wave resonances for $^{93}Nb(E_n = 35.9eV)$, $^{93}Nb(E_n = 42.3eV)$, $^{108}Pd(E_n = 2.96eV)$ and $^{124}Sn(E_n = 62.0eV)$.

We describe the details of data analysis below. The helicity of incident neutrons was flipped by reversing the magnetic field direction of the $150G$ solenoid and the $50G$ solenoid as discussed in section 3.2. Difference of photomultiplier gain between two magnetic field directions causes a false helicity dependence of γ-ray yields. We have carried out two measurements for each target to remove the false helicity dependence. The resonance components of capture γ-ray yields for incident positive- and negative-helicity neutrons can be written as

$$\begin{aligned} n_\gamma^+ &= C\Omega\eta(1 + p_n A), \\ n_\gamma^- &= C\Omega\eta'(1 - p_n A). \end{aligned} \tag{25}$$

The C is a constant common to $n_\gamma^\pm$. The Ω is the geometrical acceptance of the counter. The p_n is the polarization of incident neutrons. The A is the helicity dependent asymmetry of the resonance components of capture γ-ray counting rates. The A is different from the longitudinal asymmetry A_L due to the multiple scattering effect discussed in the latter part of this section. The η and η' are the counter efficiencies with two different magnetic field directions of the solenoids.

The η and η' were cancelled by the following procedure. The proton polarization can be reversed by changing the microwave frequency in the same magnetic field (Appendix B). When the proton polarization is reversed, the relation between neutron helicity and magnetic field is reversed, and the resonance components of capture γ-ray yields can be written as

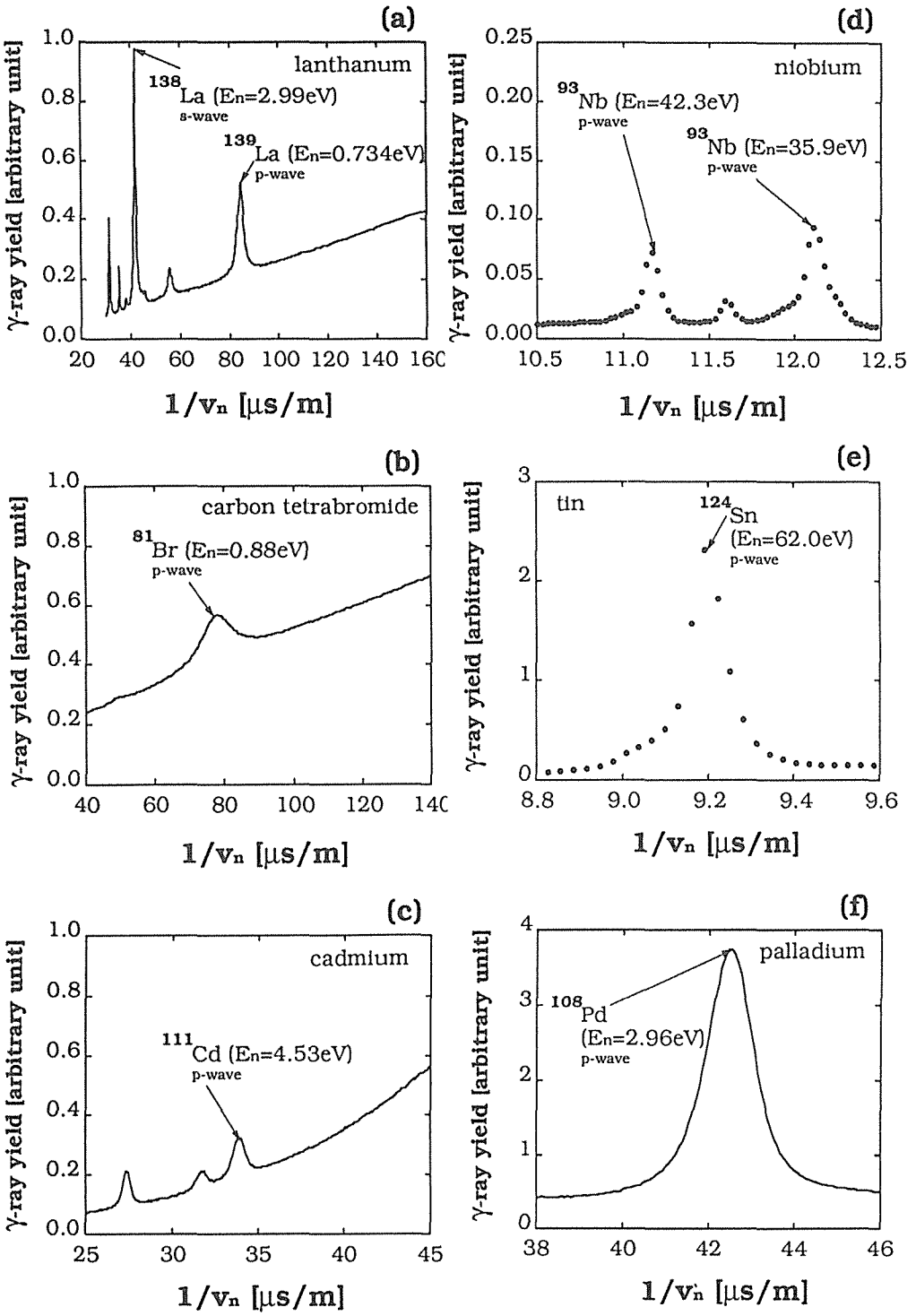

Fig. 13. The γ-ray yields versus incident neutron velocity ($1/v_n$) obtained with the BaF_2 counter discussed in section 4.1 for (a) lanthanum, (b) carbon tetrabromide, (c) cadmium, (d) niobium, (e) tin and (f) palladium targets. They are normalized by incident neutron intensity.

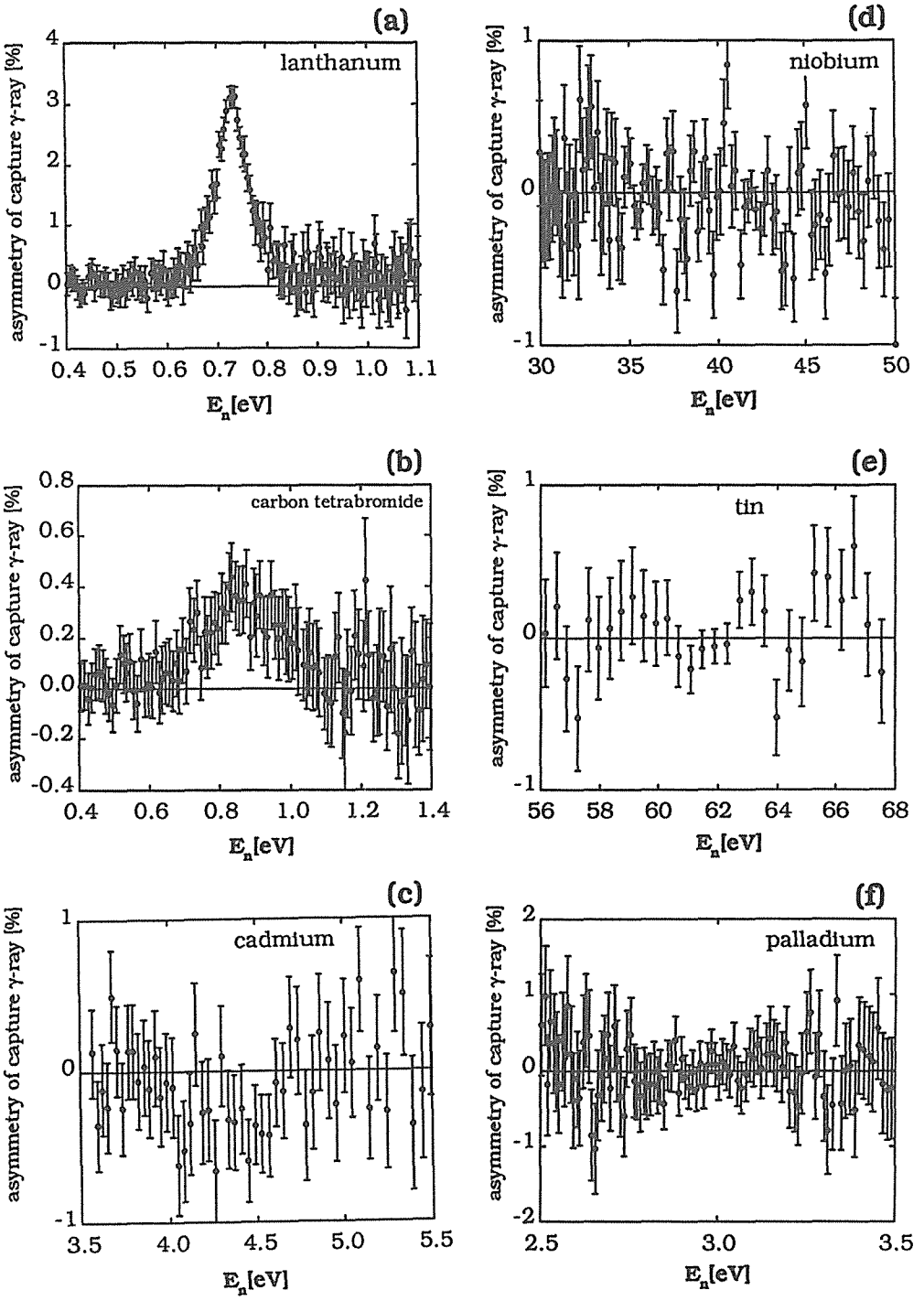

Fig. 14. The helicity dependent asymmetries of capture γ-ray yields versus incident neutron energy for (a) lanthanum, (b) carbon tetrabromide, (c) cadmium, (d) niobium, (e) tin and (f) palladium targets. The continuum components are not subtracted.

$$\begin{aligned} \bar{n}_\gamma^+ &= C\Omega\eta'(1 + \bar{p}_n A), \\ \bar{n}_\gamma^- &= C\Omega\eta(1 - \bar{p}_n A), \end{aligned} \tag{26}$$

where $\bar{p}_n$ is the incident neutron polarization in the measurement. If we define X as,

$$X = \frac{2}{p_n + \bar{p}_n} \frac{n_\gamma^+ \bar{n}_\gamma^+ - n_\gamma^- \bar{n}_\gamma^-}{n_\gamma^+ \bar{n}_\gamma^+ + n_\gamma^- \bar{n}_\gamma^-}, \tag{27}$$

the η and η' are cancelled in the X. The A can be written using X as

$$A = \frac{X}{1 + \sqrt{1 + X^2 p_n \bar{p}_n}}. \tag{28}$$

The helicity dependence A evaluated by Eq. 28 does not contain the false helicity dependence due to the difference between η and η' [5].

The A obtained by Eq. 28 contains a multiple scattering effect which comes from the finite thickness of the target. Some of incident neutrons change their helicity states by an elastic scattering, since the neutron momentum is changed in the elastic scattering, while neutron spin direction is not changed [6]. If the scattered neutron is captured by another nucleus, the helicity dependence of the γ-ray counting rate becomes small. This effect has been evaluated by a numerical simulation. We define $N(p_n, A_L)$ as the yield of capture γ-rays of a resonance component for incident neutrons whose longitudinal polarization is p_n. The $N(p_n, A_L)$ can be writen as the sum of yields of γ-rays induced by neutrons which are captured after being scattered elastically for i-times ($N_i(p_n, A_L)$).

$$N(p_n, A_L) = \sum_{i=0}^{\infty} N_i(p_n, A_L) \tag{29}$$

The $N_i(p_n, A_L)$'s were calculated by a numerical simulation (Appendix D). We define the "calculated" logitudinal asymmetry as

$$\tilde{A}(A_L) = \frac{1}{p_n} \frac{N(p_n, A_L) - N(-p_n, A_L)}{N(p_n, A_L) + N(-p_n, A_L)}. \tag{30}$$

The value of A_L was determined so that the "calculated" longitudinal asymmetry $\tilde{A}(A_L)$ reproduces the measured helicity dependent asymmetry A.

The E_n dependence of A for ^{139}La target is shown in Fig. 15 together with that of $\tilde{A}(A_L)$ where the A_L is assumed to be independent of E_n. The target was a $1.0cm$-thick lanthanum metal disk of $2.5cm$ in diameter which was cooled down to $35K$. The E_n dependence of A is well reproduced by the numerical simulation described above. The E_n dependence of A for the $0.3cm$-thick lanthanum target which was cooled down to $9K$ is also shown in Fig. 16. The E_n dependence of A is mainly due to the effect of multiple scattering inside the target, and no

[5] Experimentally, the difference between η and η' has been measured to be small ($< 10^{-3}$).

[6] The neutron spin can be flipped by the contribution of incoherent scattering. It becomes important in the analysis of forward-backward asymmetry.

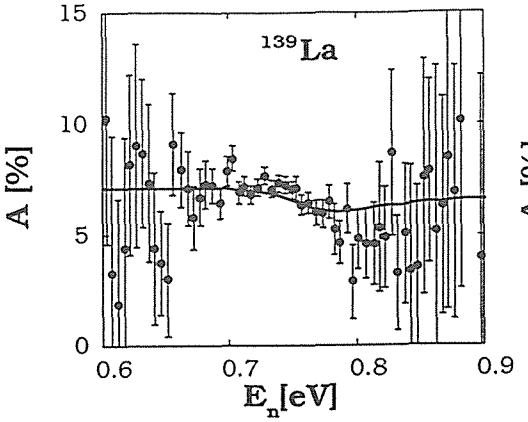

Fig. 15. The A (black circles) defined in Eq. 28 is plotted with the result of numerical simulation (solid line) where the A_L is assumed to be constant with E_n. The target was $1\,cm$ thick metal lanthanum cooled down to $35\,K$.

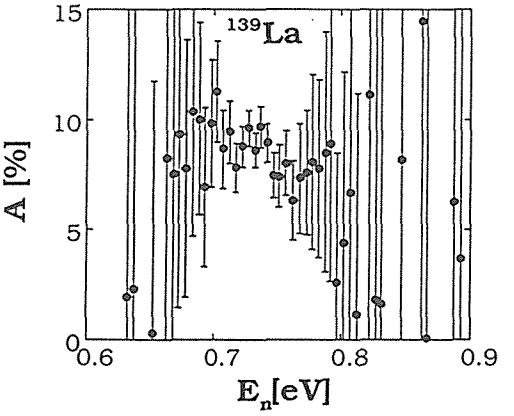

Fig. 16. The A (Eq. 28) for $0.3\,cm$ thick metal lanthanum target cooled down to $9\,K$.

significant E_n dependence of A_L has been observed.

The obtained results of A_L are listed in Table 5. The error of A consists of statistical error of γ-ray yields and the error of p_n. The error of neutron polarization (p_n) is mainly due to the uncertainty in determination of p_n using Eq. 23. The statistical error of p_n is less than 0.1 %. The statistical error of γ-ray yields is dominant except the case of a ^{139}La target. In the case of ^{139}La, the statistical error of helicity dependent asymmetry is less than 0.1 % which is smaller than the error of p_n. The A_L has been obtained after the correction of multiple scattering effects (Eq. 30) whose uncertainty is negligible.

The A_L has been studied in p-wave resonance cross sections for $^{139}La(E_n =$

Table 5. The experimental values of A_L for the p-wave resonances for several target nuclei. The energy threshold level for γ-ray detection was set to $\sim 1\,MeV$. The A_L^c is the helicity dependent asymmetry of continuum component.

target nucleus	E_n [eV]	p_n [%]	A [%]	A_L [%]		A_L^c [%]
^{81}Br	0.88	69 ± 2	1.8 ± 0.2	2.1 ± 0.2	3cm thick	-0.05 ± 0.04
		69 ± 2	1.7 ± 0.1	2.1 ± 0.2	5cm thick	0.04 ± 0.03
				2.1 ± 0.1	average	0.02 ± 0.02
^{93}Nb	35.9	46 ± 1	0.2 ± 0.2	0.3 ± 0.5		-0.05 ± 0.05
	42.3	45 ± 1	-0.0 ± 0.3	-0.0 ± 0.6		-0.05 ± 0.05
^{108}Pd	2.96	61 ± 2	0.1 ± 0.1	0.2 ± 0.2		-0.08 ± 0.10
^{111}Cd	4.53	63 ± 2	$-(1.1^{+0.5}_{-0.3})$	$-(1.3^{+0.7}_{-0.4})$		-0.07 ± 0.05
^{124}Sn	62	47 ± 1	0.1 ± 0.2	0.2 ± 0.4		-0.13 ± 0.23
^{139}La	0.734	67 ± 2	8.1 ± 0.2	9.8 ± 0.3		0.02 ± 0.04
^{138}La	2.99	63 ± 2	0.0 ± 0.1	0.0 ± 0.1	s-wave	0.00 ± 0.10

$0.734eV$), $^{81}Br(E_n = 0.88eV)$, $^{111}Cd(E_n = 4.53eV)$, $^{93}Nb(E_n = 35.9,\ 42.3eV)$, $^{108}Pd(E_n = 2.96eV)$ and $^{124}Sn(E_n = 62.0eV)$. Obtained results are $A_L = (9.8 \pm 0.3)\,\%$, $(2.1 \pm 0.1)\,\%$ and $-(1.3^{+0.7}_{-0.4})\,\%$ for ^{139}La, ^{81}Br and ^{111}Cd target nuclei, respectively, while no sizable helicity dependence has been observed for ^{93}Nb, ^{108}Pd and ^{124}Sn target nuclei. These are consistent with the results obtained at Dubna except the case of ^{139}La target nuclei.

The A_L^c listed in Table 5 is the helicity dependent asymmetries of continuum component of capture γ-rays which has been evaluated by replacing the $n_\gamma^\pm$ and $\bar{n}_\gamma^\pm$ in Eq. 25 and Eq. 26 with γ-ray yields of the continuum component obtained by the least square fitting described in the beginning of this subsection. The multiple scattering effects in A_L^c are also corrected by numerical simulations. For all the targets, the A_L^c's are zero within experimental errors.

The value of $A_L = 0.0 \pm 0.1\,\%$ has been obtained for the s-wave resonance for $^{138}La(E_n = 2.99eV)$.

The angular dependence of $a_{L,\gamma}(\theta)$ has been analyzed in the same way as described above. The helicity dependent asymmetries of capture γ-ray yields

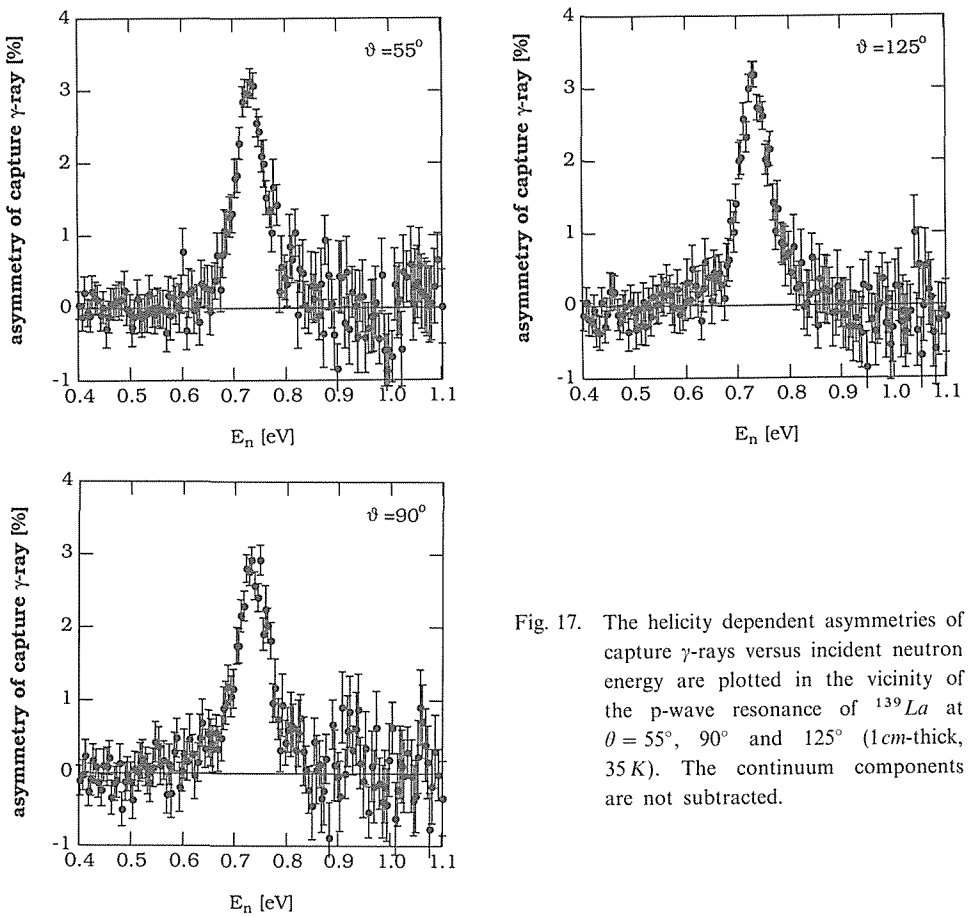

Fig. 17. The helicity dependent asymmetries of capture γ-rays versus incident neutron energy are plotted in the vicinity of the p-wave resonance of ^{139}La at $\theta = 55°$, $90°$ and $125°$ ($1cm$-thick, $35K$). The continuum components are not subtracted.

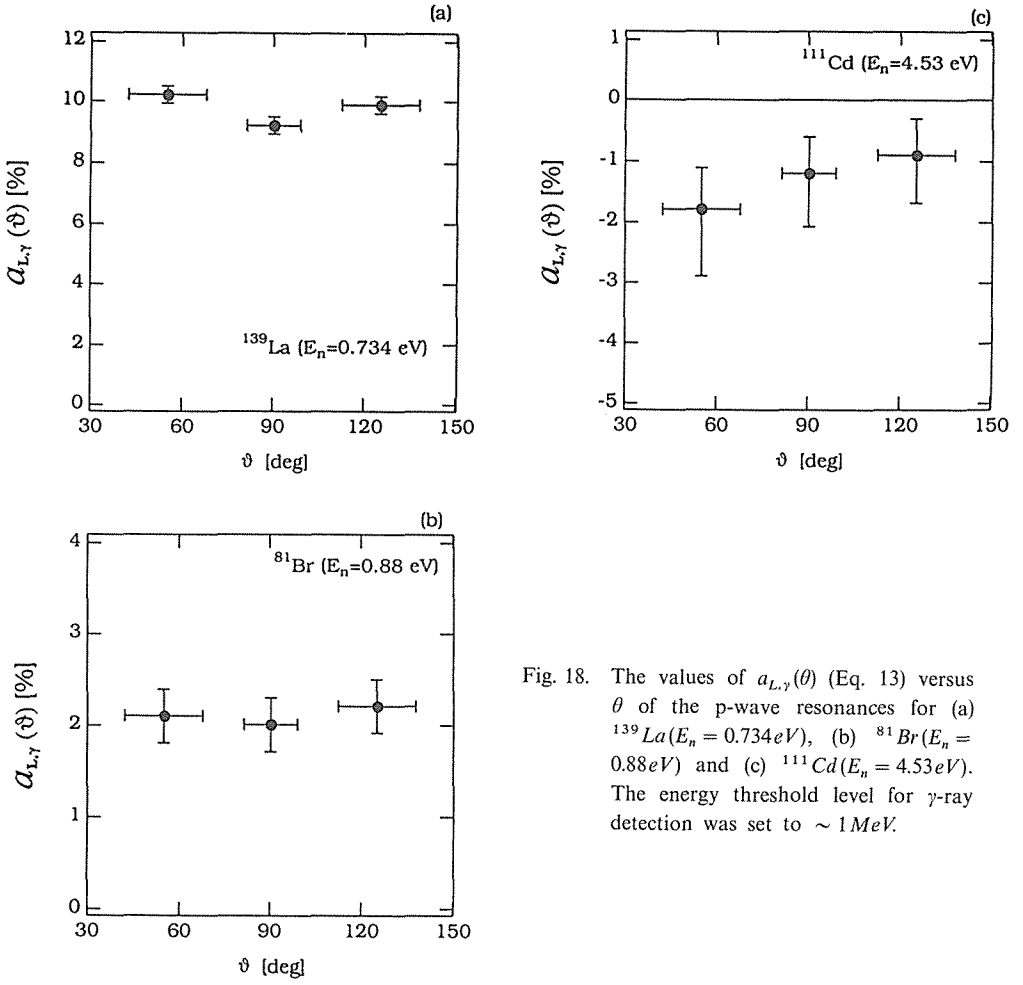

Fig. 18. The values of $a_{L,\gamma}(\theta)$ (Eq. 13) versus θ of the p-wave resonances for (a) $^{139}La(E_n = 0.734eV)$, (b) $^{81}Br(E_n = 0.88eV)$ and (c) $^{111}Cd(E_n = 4.53eV)$. The energy threshold level for γ-ray detection was set to $\sim 1MeV$.

measured at $\theta = 55°$, $90°$ and $125°$ versus incident neutron energy are shown in Fig. 17 for lanthanum target. The $a_{L,\gamma}(\theta)$ in p-wave resonances for ^{139}La, ^{81}Br and ^{111}Cd target nuclei is plotted in Fig. 18. In all cases, the $a_{L,\gamma}(\theta)$ has been found to be independent of θ within experimental errors.

5.2 Angular Distribution

The angular distribution of capture γ-rays induced by incident unpolarized neutrons has been measured. The angular distribution observed in the measurement contains false angular distribution due to the finite thickness of the target; (1) the attenuation of the γ-ray inside the target, (2) the inhomogeneous distribution of the reaction point due to the neutron attenuation in the target, and (3) capture of neutrons scattered by another target nucleus. The false angular distribution has been evaluated by numerical simulations. The uncertainty in determination of α_{01} and α_{02} due to the γ-ray energy dependence of the mean free path was added to

experimental errors. The error due to the uncertainty is comparable with statistical errors of γ-ray yields. The results are plotted in Fig. 19 with the best fit curves. The obtained values of α_{01} and α_{02} are listed in Table 6.

The angular distribution of the s-wave resonance of ^{107}Ag target ($E_n = 16.30eV$) has been observed to be uniform.

Combining these results with the results of $a_{L,\gamma}(\theta)$ discussed in the previous subsection, all the parameters in Eq. 10 have been determined in the p-wave

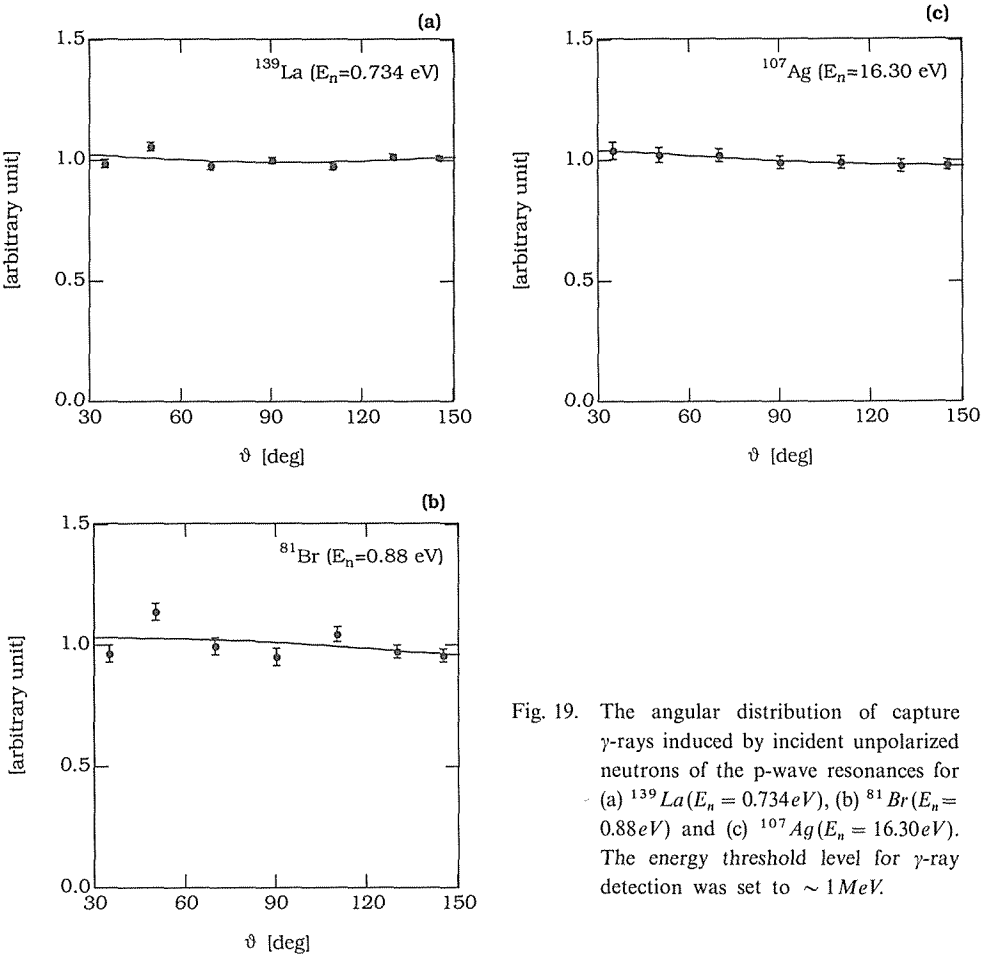

Fig. 19. The angular distribution of capture γ-rays induced by incident unpolarized neutrons of the p-wave resonances for (a) $^{139}La(E_n = 0.734eV)$, (b) $^{81}Br(E_n = 0.88eV)$ and (c) $^{107}Ag(E_n = 16.30eV)$. The energy threshold level for γ-ray detection was set to $\sim 1MeV$.

Table 6. The experimental values of α_{01} and α_{02}. The energy threshold level for γ-ray detection was set to $\sim 1MeV$.

target nucleus	E_n [eV]	α_{01} [%]	α_{02} [%]
^{139}La	0.734	-1.3 ± 3.1	2.1 ± 2.3
^{81}Br	0.88	-1.7 ± 2.7	3.0 ± 4.1
^{107}Ag	16.30	-0.7 ± 2.0	-0.9 ± 2.0

Table 7. The experimental values of the parameters given in Eq. 10. The energy threshold level for γ-ray detection was set to $\sim 1 MeV$.

target nucleus	E_n [eV]	α_{01} [%]	α_{02} [%]	A_L [%]	α_{L1} [%]	α_{L2} [%]
^{139}La	0.734	-1.3 ± 3.0	2.1 ± 2.4	10.1 ± 0.7	0.1 ± 1.2	2.9 ± 3.8
^{81}Br	0.88	-1.7 ± 3.0	2.8 ± 4.2	2.2 ± 0.7	-0.5 ± 1.2	0.1 ± 3.8

resonances for ^{139}La and ^{81}Br target nuclei. The results are listed in Table 7. All of the angular dependent terms are consistent with zero within experimental errors, while the A_L is very large.

5.3 The E_γ Dependence of Longitudinal Asymmetry

The longitudinal asymmetry A_L has been measured with different energy threshold levels for γ-ray detection with a better energy resolution using the BGO counter described in section 4.3. The counter was designed to detect the γ-rays at $\theta \simeq \theta_0$, $\pi - \theta_0$ so that the A_L can be evaluated following the Eq. 15. Multiple scattering effects are evaluated in the same way as discussed in section 5.1.

The obtained results are listed in Table 8 and plotted in Fig. 20. The $E_{\gamma,thres}$

Table 8. The experimental values of A_L of the p-wave resonance for ^{139}La target nuclei ($E_n = 0.734eV$) obtained with different energy threshold levels for γ-ray detection ($E_{\gamma,thres}$). The A_L^c is the helicity dependent asymmetry of continuum component.

$E_{\gamma,thres}$ [MeV]	p_n [%]	A [%]	A_L [%]	A_L^c [%]
1.1 ± 0.1	63 ± 2	7.2 ± 0.2	9.4 ± 0.3	-0.02 ± 0.03
3.2 ± 0.2	65 ± 2	7.1 ± 0.2	9.3 ± 0.2	0.04 ± 0.04
4.2 ± 0.2	65 ± 2	7.7 ± 0.5	9.9 ± 0.7	-0.04 ± 0.07
4.8 ± 0.3	67 ± 2	7.3 ± 1.4	9.5 ± 1.9	0.22 ± 0.18

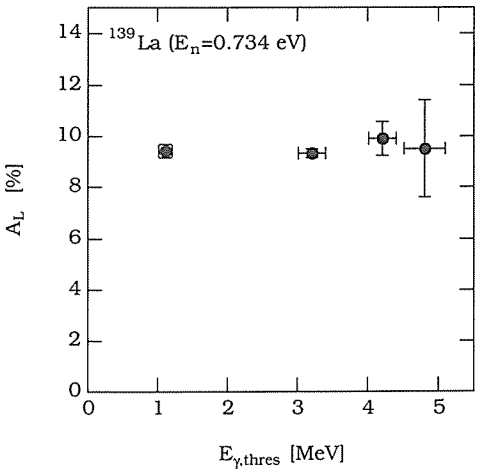

Fig. 20. The A_L versus $E_{\gamma,thres}$ in the p-wave resonance for $^{139}La(E_n = 0.734eV)$.

represents the energy threshold level for γ-ray detection. The error of neutron polarization (p_n) is mainly due to the uncertainty in determination of p_n using Eq. 23. The statistical error of p_n is negligible (less than 0.1 %). The statistical errors of A are negligible compared with errors of p_n for $E_{\gamma,thres} = 1.1$ and $3.2 MeV$. In the case of $E_{\gamma,thres} = 4.2 MeV$, the error of p_n is almost equal to the statistical errors of A. In the case of $E_{\gamma,thres} = 4.8 MeV$, the error of p_n is smaller than the statistical errors of A. The asymmetries of the continuum component of capture γ-rays with respect to the helicity of incident neutrons (A_L^c) are also listed in the table. No significant helicity dependence which exceeds experimental errors has been found in the continuum components. The longitudinal asymmetry of the s-wave resonance for $^{138}La(E_n = 2.99 eV)$ have been found to be less than 0.3 %.

The forward-backward asymmetry (a_γ) given by Eq. 17 has been also measured in the same measurement. The γ-rays were detected at two angles (θ and $\pi - \theta$). Following notations in section 5.1, the γ-ray yields can be written as

$$\begin{aligned} n_\gamma^+(\theta) &= C\Omega_F\eta_F(1 + p_nA)(1 + p_na\cos\theta), \\ n_\gamma^-(\theta) &= C\Omega_F\eta'_F(1 - p_nA)(1 - p_na\cos\theta), \\ n_\gamma^+(\pi - \theta) &= C\Omega_B\eta_B(1 + p_nA)(1 - p_na\cos\theta), \\ n_\gamma^-(\pi - \theta) &= C\Omega_B\eta'_B(1 - p_nA)(1 + p_na\cos\theta), \end{aligned} \tag{31}$$

where a is forward-backward asymmetry of γ-ray yields. The Ω_F and Ω_B are the geometrical acceptances of the counters at θ and $\pi - \theta$, respectively. The a in Eq. 31 has been evaluated after cancelling η's in a similar way to the method discussed in section 5.1.

The a in Eq. 31 contains a multiple scattering effect. The neutron polarization becomes $(1 - 4R/3)$ times of original polarization due to the incoherent scattering on every elastic scattering [61], where $R = \sigma_{incoh}/(\sigma_{incoh} + \sigma_{coh})$. The σ_{coh} and σ_{incoh} are coherent- and incoherent- scattering cross sections, respectively. Therefore, the polarization of incident neutrons becomes p'_n effectively, where p'_n is given as

$$p'_n = p_n \frac{\sum_i N_i \left(1 - \frac{4}{3}R\right)^i}{\sum_i N_i}, \tag{32}$$

where $N_i = (N_i^+ + N_i^-)/2$. The $N_i^\pm$ is given in section 5.1 (Eq. 29). The a_γ was evaluated from the following relation.

$$p_n a = p'_n a_\gamma \tag{33}$$

The obtained results of $a_{\gamma,\langle}$, $a_{\gamma,\rangle}$, $a_{\gamma,\langle\rangle}$ and $\langle a_\gamma \rangle$ (see section 2) are listed in Table 9 for the cases of $E_{\gamma,thres} = 1.1 \pm 0.1 MeV$ and $4.8 \pm 0.3 MeV$. Statistical errors of γ-ray yields are dominant in the experimental errors, and other errors are negligible. In both cases, the forward-backward asymmetry of the continuum component has been found to be less than 0.3 %. The $\langle a_\gamma \rangle$ of the s-wave resonance

Table 9. The experimental values of the forward-backward asymmetry of the p-wave resonance for ^{139}La target ($E_n = 0.734eV$) obtained with low and high energy threshold levels for γ-rays

$E_{\gamma,thres}$ [MeV]	$a_{\gamma,<}$ [%]	$a_{\gamma,>}$ [%]	$a_{\gamma,<>}$ [%]	$\langle a_\gamma \rangle$ [%]
1.1 ± 0.1	-0.1 ± 0.4	-0.2 ± 0.3	-0.2 ± 0.2	0.1 ± 0.3
4.8 ± 0.3	3.3 ± 1.4	-6.1 ± 4.0	-1.8 ± 2.7	4.7 ± 2.1

for ^{138}La ($E_n = 2.99eV$) has been observed to be less than 0.2 %.

6 Theoretical Interpretation

In this section, the mechanism which is responsible for a large PNC effect in n-A interactions is discussed in the context of interference between s- and p-wave resonance components.

We assume that all the processes in this energy region can be described by the contributions of s- and p-wave component of incident neutrons [7], and that only an s-wave resonance and a p-wave resonance exist in the energy region of our interest.

Total Hamitonian of a compound nucleus consists of a PC part (H_{PC}) and a PNC part (H_{PNC}). The s- and p-wave compound states represented by $|s\rangle$ and $|p\rangle$, are mixed up by a small non-orthogonal component H_{PNC}. The mixed states $|s'\rangle$ and $|p'\rangle$ can be written as

$$\begin{aligned} |s'\rangle &= |s\rangle - \frac{\langle s|H_{PNC}|p\rangle}{E_p - E_s}|p\rangle, \\ |p'\rangle &= |p\rangle + \frac{\langle s|H_{PNC}|p\rangle}{E_p - E_s}|s\rangle, \end{aligned} \tag{34}$$

in the first order perturbation, where E_s and E_p are resonance energies of s- and p-wave resonances.

The A_{10} ($= A_L$, see Eq. 11) is given as [29, 48],

$$A_{10} \sim -\frac{2W}{E_p - E_s}\sqrt{\frac{\Gamma_s^n}{\Gamma_p^n}}\,\eta_{p\frac{1}{2}}\sqrt{\frac{\Gamma_{p\frac{1}{2}}^n}{\Gamma_p^n}}, \tag{35}$$

where $W = i\langle s|H_{PNC}|p\rangle$, and Γ_s^n and Γ_p^n are neutron widths of s- and p-wave resonances. The $\Gamma_{p\frac{1}{2}}^n$ is the partial neutron width of p-wave resonance for $j = 1/2$ incident neutrons, where j is the total angular momentum of incident neutrons. The $\eta_{p\frac{1}{2}}$ is the sign factor of the reduced T-matrix element (see Eq. (A-5) in Appendix A). Two kinds of mechanisms are responsible for the large PNC effect. One is

[7] Another approach based on the interference between p- and d-wave component is argued to explain the large PNC effects [30, 31].

"dynamical enhancement" ($W/(E_p - E_s)$), and the other is "structural enhancement" ($\sqrt{\Gamma_s^n/\Gamma_p^n}$). The factor $\sqrt{\Gamma_{p\frac{1}{2}}^n/\Gamma_p^n}$ is not responsible for the large PNC effect.

The "dynamical enhancement" arises from a statistical nature of a compound state. A typical time scale of a capture reaction through a compound state is $\hbar/\Gamma \sim 10^{-14}s$ for $\Gamma \sim 0.1eV$, while that of a direct process is given by the time in which a neutron passes through a nucleus, that is, $2R/v_n \sim 10^{-18}s$ for $E_n \sim 1eV$, where $R \sim 10fm$ is a typical nuclear radius. The nucleons have much longer time to interact with each other in the compound state than in the direct process. Small PNC effects in N-N interaction are accumulated during the long life time as discussed below [29]. The s- and p-wave compound states ($|s\rangle$ and $|p\rangle$) can be expanded by a number of single particle-hole states in a nuclear shell model as

$$|s\rangle = \sum_i^N a_i|\phi_i\rangle, \qquad |p\rangle = \sum_i^N b_i|\phi_i'\rangle. \tag{36}$$

The magnitudes of the coefficients a_i and b_j are the order of $1/\sqrt{N}$ because of the normalization conditions of $|s\rangle$ and $|p\rangle$. If we write a scale of excitation energies of single particle-hole states as ΔE and an average level spacing of compound states as D, the number N is given as

$$N \sim \frac{\Delta E}{D}. \tag{37}$$

If we use typical values of $\Delta E \sim 10^6 eV$ and $D \sim 10eV$, we obtain $N \sim 10^5$. The magnitude of PNC matrix element W in compound state is expressed as

$$|W| = |\langle s|H_{PNC}|p\rangle| = |\langle \sum_i a_i\phi_i|H_{PNC}|\sum_j b_j\phi_j'\rangle| = |\sum_{i,j} a_i^* b_j\langle\phi_i|H_{PNC}|\phi_j'\rangle|. \tag{38}$$

It is natural to assume the signs of a_i and b_j appear at random. Therefore, the $|W|$ is given as

$$|W| \sim \frac{|\langle H_{PNC}\rangle|}{N} \times \sqrt{N}, \tag{39}$$

and it leads to

$$\left|\frac{W}{E_p - E_s}\right| \sim \frac{|W|}{D} \sim \frac{|\langle H_{PNC}\rangle|}{\sqrt{N}} \frac{1}{\frac{\Delta E}{N}} = \frac{|\langle H_{PNC}\rangle|}{\Delta E}\sqrt{N}, \tag{40}$$

where the $\langle H_{PNC}\rangle$ is the average value of the $\langle\phi_i|H_{PNC}|\phi_i'\rangle$. The factor $|\langle H_{PNC}\rangle/\Delta E|$ is a typical size of parity mixing in single particle states which is the same order as that of N-N interaction (α_{NN}). The small PNC effect in N-N interaction is accumulated up to $\sqrt{N} = 10^2 \sim 10^3$ times.

The "structural enhancement" arises from the difference of the centrifugal potential barriers between s- and p-wave incident neutrons. The s- and p-wave

neutron widths (Γ_s^n and Γ_p^n) are

$$\Gamma_s^n \propto k_n R, \qquad \Gamma_p^n \propto (k_n R)^3, \tag{41}$$

and the structural enhancement factor is given as

$$\sqrt{\frac{\Gamma_s^n}{\Gamma_p^n}} \sim \frac{1}{k_n R}. \tag{42}$$

The neutron momentum k_n is $\sim 2 \times 10^{-4} fm^{-1}$ for $1eV$ neutrons. If we use a typical value of $R \sim 10fm$, we obtain $\sqrt{\Gamma_s^n/\Gamma_p^n} \sim 10^3$.

From these two mechanisms, the PNC effect in a compound state becomes $10^5 \sim 10^6$ times larger than the PNC effect in N-N interaction.

Here we discuss the remained factor $\sqrt{\Gamma_{p\frac{1}{2}}^n/\Gamma_p^n}$. The total angular momentum of compound state $\vec{J}$ is the sum of the target nucleus spin $\vec{I}$, the neutron spin $\vec{s}$ ($s = 1/2$) and the orbital angular momentum $\vec{l}$ ($l = 0$ or 1). We sum the angular momenta in the following order.

$$\vec{J} = \vec{I} + \vec{j}, \qquad \vec{j} = \vec{s} + \vec{l} \tag{43}$$

The vector $\vec{j}$ is the total angular momentum of the incident neutron. The absolute value of $\vec{j}$ is given as

$$\begin{aligned} j &= \tfrac{1}{2} && \text{for s-wave,} \\ j &= \tfrac{1}{2} \quad \text{or } \tfrac{3}{2} && \text{for p-wave.} \end{aligned}$$

In the case of $I = 0$, $\vec{J}$ is equal to $\vec{j}$, and the $j = 3/2$ component of p-wave does not interfere with an s-wave component, since its total angular momentum is different from that of an s-wave component. It can be generalized to the cases of $I \neq 0$ and the factor $\sqrt{\Gamma_{p\frac{1}{2}}^n/\Gamma_p^n}$ gives the interfering part out of all p-wave contributions. We define x and y as

$$x = \eta_{p\frac{1}{2}} \sqrt{\frac{\Gamma_{p\frac{1}{2}}^n}{\Gamma_p^n}}, \qquad y = \eta_{p\frac{3}{2}} \sqrt{\frac{\Gamma_{p\frac{3}{2}}^n}{\Gamma_p^n}}, \tag{44}$$

where $\Gamma_p^n = \Gamma_{p\frac{1}{2}}^n + \Gamma_{p\frac{3}{2}}^n$. The η_{pj}'s are sign factors (see Eq. (A-5) in Appendix A). The absolute value of x cannot exceed unity because of the relation of $x^2 + y^2 = 1$. The x does not contribute to enlarge the PNC effect.

Explicit expressions of other terms in Eq. 11 in the vicinity of the p-wave resonance for a single γ-ray transition are discussed below (see Ref. [48] and Appendix A). Intrinsic parities of the compound state and the final state are assumed to be the same. The dominant parity-favored transition is an M1

transition while the dominant parity unfavored one is E1. The A_i's defined in section 2 are given as

$$A_1 \sim \eta_\gamma \frac{1}{(E_p - E_s)} \sqrt{\frac{\Gamma_s^n}{\Gamma_p^n} \frac{\Gamma_{M1}}{\Gamma_{E1}}} (E_n - E_p) \sum_j \xi_j P(J_s J_p \tfrac{1}{2} j 1 IF), \tag{45}$$

$$A_3 = 3\sqrt{10} \sum_{jj'} \xi_j \xi_{j'} P(J_p J_p jj' 2 IF) \begin{Bmatrix} 2 & 1 & 1 \\ 0 & \frac{1}{2} & \frac{1}{2} \\ 2 & j & j' \end{Bmatrix}, \tag{46}$$

$$A_9 \sim -2\eta_\gamma \frac{W}{(E_p - E_s)^2} \frac{\Gamma_s^n}{\Gamma_p^n} \sqrt{\frac{\Gamma_{M1}}{\Gamma_{E1}}} (E_n - E_p) P(J_s J_s \tfrac{1}{2} \tfrac{1}{2} 1 IF), \tag{47}$$

$$A_{11} \sim \sqrt{3} y \frac{W}{E_p - E_s} \sqrt{\frac{\Gamma_s^n}{\Gamma_p^n}} P(J_s J_p \tfrac{1}{2} \tfrac{3}{2} 2 IF), \tag{48}$$

$$A_{12} \sim -36\eta_\gamma \frac{W}{E_p - E_s} \sqrt{\frac{\Gamma_{M1}}{\Gamma_{E1}}} \sum_{jj'} \xi_j \xi_{j'} P(J_p J_p jj' 1 IF) \begin{Bmatrix} 2 & 1 & 1 \\ 1 & \frac{1}{2} & \frac{1}{2} \\ 1 & j & j' \end{Bmatrix}, \tag{49}$$

in the vicinity of the p-wave resonance, where J_s, J_p and F are spins of the s-wave resonance, p-wave resonance and final state, respectively. The Γ_{M1} and Γ_{E1} are widths of the M1 and E1 transitions. The $\eta_\gamma = \pm 1$ [48] is a sign factor and we define the ξ_j and the function P as

$$\xi_j = \begin{cases} x & \text{for } j = \frac{1}{2}, \\ y & \text{for } j = \frac{3}{2}, \end{cases} \tag{50}$$

$$P(JJ'jj'kIF) = (-1)^{J+J'+j'+I+F} \frac{3}{2} \sqrt{(2J+1)(2J'+1)} \begin{Bmatrix} k & j & j' \\ I & J' & J \end{Bmatrix} \begin{Bmatrix} k & 1 & 1 \\ F & J' & J \end{Bmatrix}. \tag{51}$$

The A_i's are classified into two types of E_n dependence. The A_3, A_{10}, A_{11} and A_{12} are constant functions of E_n in the vicinity of the p-wave resonance while the A_1 and A_9 change their signs at $E_n = E_p$. The values of A_i's of the former type can be discussed at $E_n = E_p$ while those of the latter type must be discussed at $E_n = E_p \pm \Gamma_p/2$. The A_{10} contains no quantity which depends on γ-ray transitions. Therefore the A_{10} is predicted to be independent of γ-ray transitions. On the other hand, other A_i's contain quantities which depend on γ-ray transitions, those are, the sign factor η_γ, the function P, the 9-j symbol and the factor $\sqrt{\Gamma_{M1}/\Gamma_{E1}}$. If a number of γ-ray transitions are detected with low energy threshold levels without identification of individual γ-ray transitions, the contributions of γ-ray transitions cancel each other since they have different signs and magnitudes, and the A_i's become very small except A_{10}.

In a measurement of single γ-ray transition, large values of A_i's which depend on

γ-ray transitions can be observed if the size of the factor $\sqrt{\Gamma_{M1}/\Gamma_{E1}}$ $(=10^{-2}\sim 10^{2})$ is not very small.

7 Discussion

In this section, we discuss the properties of a large PNC effect in a $(\vec{n}, \gamma)$ reaction for ^{139}La target nuclei and the origin of large values of A_L in p-wave resonances for several target nuclei. We mention a PNC effect in the exit channel for $^{139}La(\vec{n}, \gamma)$ reaction in the latter part of this section.

We have studied properties of the helicity dependence of capture γ-ray intensity in the p-wave resonance for $^{139}La\,(E_n = 0.734eV)$.

$\langle E_\gamma$ **dependence of** $A_L\rangle$ The longitudinal asymmetry A_L has been measured with several energy threshold levels for γ-ray detection. It has been found that the value of A_L is independent of γ-ray energy within experimental errors. The large A_L has no immediate connection with the PNC effect of exit channels. It implies that the large longitudinal asymmetry is caused by entrance-channel parity-mixing between two opposite-parity amplitudes.

$\langle\theta$ **dependence**$\rangle$ All the parameters which appear in radiative capture reactions induced by longitudinally polarized incident neutrons (see Eq. 10) have been determined in the measurement with $1MeV$ γ-ray energy threshold levels by measuring the angular dependence of $a_{L,\gamma}(\theta)$ (Eq. 13) and angular distribution of capture γ-rays induced by unpolarized neutrons. The angular dependent terms (α's) have been found to be zero within experimental errors, while the A_L term has a large value. The α's which contain the exit-channel parity-mixing are very small in the measurement with $1MeV$ γ-ray energy threshold levels. It implies that the contributions of many γ-raytransitions cancel each other.

The discrepancy between the results obtained at Dubna and KEK (see section 1) cannot be explained by the contribution of angular dependent terms.

$\langle E_n$ **dependence of** $A_L\rangle$ It has been found that A_L is independent of E_n within the resonance width in the case of lanthanum target, which was cooled down to $35K$ and $9K$. At these temperatures, the Doppler broadening does not affect the neutron energy resolution. It is consistent with Eq. 35 which is derived based on the interference between s- and p-wave components. [8]

The large PNC effects are consistent with the theory based on the parity mixing in an entrance channel discussed in section 6. It is important for the TRI experiment in neutron transmission method. If the large PNC effects are due to the exit-channel parity mixing, we must observe contributions of individual γ-ray transitions separately where large FSI effects are expected.

All parameters in Eq. 10 have been determined also in the p-wave resonance

[8]The results are also consistent with another theoretical approach based on the interference between p- and d-wave components.

for ^{81}Br ($E_n = 0.88eV$) in the measurement with $1MeV$ γ-ray energy threshold levels. Only the A_L term has a large value, while all the angular dependent terms have been found to be zero within experimental errors. The angular dependence of $a_{L,\gamma}(\theta)$ has been studied also in the p-wave resonance for ^{111}Cd ($E_n = 4.53eV$) in the measurement with $1MeV$ γ-ray energy threshold levels, and no sizable angular dependence has been observed.

The γ-ray detection method is a very efficient method to study a large PNC effect since it is insensitive to potential scatterings where no large PNC is expected as discussed in section 1. But the contribution of angular dependent terms may exist in (n, γ) cross section. We have experimentally confirmed that the angular dependent terms are very small in the measurement with $1MeV$ γ-ray energy threshold levels since contributions of many γ-ray transitions cancel out the angular dependences. Furthermore, values of A_L measured by γ-ray detection method are consistent with those measured by neutron transmission method [9]. We can conclude the measurement of longitudinal asymmetry with such γ-ray detection has been established to be an efficient method to study large PNC effects in n-A interactions.

The angular dependent terms introduce a possibility to investigate the details of reaction mechanism which is responsible for large PNC effects.

The forward-backward asymmetry, which contains exit-channel parity-mixing, has been measured in the p-wave resonance for ^{139}La target nuclei in the γ-ray energy region higher than $1.1 \pm 0.1MeV$ where many γ-ray transitions contribute. The obtained value is $\langle a_\gamma \rangle = 0.1 \pm 0.3\,\%$. On the other hand, the $\langle a_\gamma \rangle$ measured in the γ-ray energy region higher than $4.8 \pm 0.3MeV$, where only one or two γ-ray transitions are dominant, is $\langle a_\gamma \rangle = 4.7 \pm 2.1\,\%$. The result suggests the existence of exit-channel parity-mixing in a single γ-ray transition. If we assume that the $\langle a_\gamma \rangle$ is caused by a single γ-ray transition of $^{140}La(4^- \to 4^-)$, the value of $\sqrt{\Gamma_{M1}/\Gamma_{E1}}$ is obtained from the following relation between A_{10} and A_9 (see Eq. 35 and Eq. 47).

$$\left|\frac{\langle a_\gamma \rangle}{A_L}\right| \sim \frac{|A_9|_{E_n = E_p \pm \Gamma_p/2}}{|A_{10}|_{E_n = E_p}} \sim \frac{1}{|x|} \frac{\Gamma_p}{2|E_p - E_s|} \sqrt{\frac{\Gamma_s^n}{\Gamma_p^n}} \sqrt{\frac{\Gamma_{M1}}{\Gamma_{E1}}} \, |P(44\tfrac{1}{2}\,\tfrac{1}{2}\,1\tfrac{7}{2}4)| \qquad (52)$$

Substituting the experimental values, we obtain $\sqrt{\Gamma_{M1}/\Gamma_{E1}} \sim 5.6 \pm 2.5$ assuming $|x| = 1$. But if another γ-ray transition of $^{140}La(4^- \to 5^-)$ contributes to the $\langle a_\gamma \rangle$, exit-channel structural enhancement factor should be different. Further study is necessary to examine the parity-mixing in exit channels.

The A_L has been measured in p-wave resonances of ^{81}Br, ^{93}Nb, ^{108}Pd, ^{111}Cd, ^{124}Sn and ^{139}La target nuclei by a γ-ray detection method with $1MeV$ energy threshold. We re-examine the results of A_L in the framework of the parity-mixing

[9] The exception is the result obtained at Dubna for ^{139}La target.

between an s- and a p-wave resonances. We do not discuss the cases of heavy nuclei here, since the level spacing is too small to assume that the parity-mixing is caused by two separate resonances. In order to discuss the origin of the large PNC effect, it is convenient to define α_{nA} as

$$\alpha_{nA} = \frac{2}{E_p - E_s} \sqrt{\frac{\Gamma_s^n}{\Gamma_p^n}}. \tag{53}$$

Resonance parameters are listed in Table 10 with experimental values of the A_L and calculated values of $|\alpha_{nA}|$. The magnitudes of xW are shown in the rightmost column. They are obtained by substituting our experimental results into the following relation.

$$|A_L| = |xW|\,|\alpha_{nA}| \tag{54}$$

The values of $|W|$ for the p-wave resonances of $^{139}La(E_n = 0.734eV)$, $^{81}Br(E_n = 0.88eV)$ and $^{111}Cd(E_n = 4.53eV)$ are in the same order of magnitude, if we assume $|x| = 1$. The $|A_L|$ is roughly proportional to $|\alpha_{nA}|$. The large PNC effects are mainly caused by the large $|\alpha_{nA}|$.

A pair of s- and p-wave resonances which are located closely does not always cause a large PNC effect. No large PNC effect has been observed in p-wave resonances of $^{124}Sn(E_n = 62.0eV)$, $^{93}Nb(E_n = 35.9eV)$ and $^{93}Nb\,(E_n = 42.3eV)$, since their $|\alpha_{nA}|$'s are very small compared with ^{139}La, ^{81}Br and ^{111}Cd.

No PNC effect has been found in the case of the p-wave resonance for ^{108}Pd target ($E_n = 2.96eV$), in spite of the fact that α_{nA} is large, that is $7.8 \pm 0.3eV^{-1}$, if the resonance at $E_n = 33.10eV$ is taken as the neighboring s-wave resonance. The total angular momentum of the p-wave resonance is 3/2, while that of the neighboring s-wave resonance is 1/2. Two opposite-parity amplitudes connot interfere if their total angular momenta are different.

The fact that the large PNC effects are observed for only a few nuclei, can be explained as follows. Very large enhancement of a PNC effect seems to occur

Table 10. Resonance parameters and spins of compound states are listed for p-wave resonances and their neighboring s-wave resonances. The nearest s-wave resonances from p-wave resonances are taken as neighboring s-wave resonances. The g is the statistical weight factor given as $g = \dfrac{2J+1}{2(2I+1)}$. The $\Gamma_s^{n0} = \Gamma_s^n \sqrt{1eV/E_s}$ is the reduced neutron width at $1eV$ for s-wave neutrons [62, 23]. The values of $|\alpha_{nA}|$ calculated by substituting the resonance parameters into Eq. 53 are shown. The values of A_L are the experimental results obtained in this work. The values of $|xW|$ are shown in the rightmost column.

target nucleus	E_p [eV]	$2g\Gamma_p^n$ [meV]	E_s [eV]	$2g\Gamma_s^{n0}$ [meV]	J_p	J_s	A_L	$\lvert\alpha_{nA}\rvert$ [eV^{-1}]	$\lvert xW\rvert$ [meV]
^{81}Br	0.88 ± 0.01	0.000116 ± 0.000006	101.10 ± 0.14	20	unknown	unknown	0.021 ± 0.001	8.0 ± 0.2	2.6 ± 0.1
^{93}Nb	35.9 ± 0.1	0.112 ± 0.010	119.2 ± 0.2	0.37	5	5	0.003 ± 0.005	0.11 ± 0.01	
^{93}Nb	42.3 ± 0.1	0.0865 ± 0.0050	-105.39	33.24	4	4	-0.000 ± 0.006	0.68 ± 0.02	
^{108}Pd	2.96 ± 0.01	0.01008 ± 0.00010	33.10 ± 0.17	40.6 ± 2.8	$\frac{3}{2}$	$\frac{1}{2}$	0.002 ± 0.002	7.8 ± 0.3	
^{111}Cd	4.53 ± 0.03	0.00326 ± 0.00010	-4	1.9	unknown	0	$-(0.013^{+0.007}_{-0.004})$	8.3 ± 0.3	$1.6^{+0.9}_{-0.5}$
^{124}Sn	62.0 ± 0.1	14.4 ± 0.4	-20	0.30	$\frac{1}{2}$	$\frac{1}{2}$	0.002 ± 0.004	0.010 ± 0.003	
^{139}La	0.734 ± 0.005	0.000073 ± 0.000010	-48.63	168	unknown	4	0.098 ± 0.003	57 ± 4	1.7 ± 0.1

only when Γ_p^n is very small (see Table 10). In such a case, the cross section of the p-wave resonance is too small to be observed among a number of large s-wave resonances unless the p-wave resonance is well-separated from other s-wave resonances. The nucleus which has a well-separated p-wave resonance is rarely to be found. As the average level spacings of the targets of ^{139}La and ^{81}Br are $D_0 = 208 \pm 10eV$ and $94 \pm 15eV$, respectively, a well-separated resonance is likely to be found [10].

In summary, the properties of large PNC effects in n-A interactions have been studied in $(\vec{n}, \gamma)$ reactions for several nuclei. The phenomena can be explained by the interference between two opposite parity amplitudes of compound resonances in their entrance channels. They are very important candidates which can be applied to TRI test experiments.

8 Future Prospects

In this section, we point out several possibilities of further study of PNC effects. Feasibility of a TRI experiment to measure a T-odd triple vector correlation term in a neutron transmission is pointed out in the latter part of this section.

If the magnitude of the nuclear weak matrix element $|W|$ is almost in the same order for all nuclei, we can predict the value of PNC effect. For example, the A_L for $^{93}Nb\,(E_n = 42.3eV)$ must be around a few times 10^{-3}. It is very important to study the magnitude of the nuclear weak matrix element for a number of p-wave resonances in various nuclei and to confirm the assumption that the magnitude of nuclear weak matrix element is almost in the same order for all nuclei [11]. Very precise data of neutron cross sections are necessary to predict a magnitude of a PNC effect. Especially the data for small p-wave resonances are desirable, since large PNC effects have been found only in p-wave resonances which are well-separated from other resonances and have small neutron widths. Assignments of the total angular momentum and the orbital angular momentum of incident neutrons are also necessary.

For further understanding of the reaction mechanism which is responsible for large PNC effects, we can study exit-channel parity-mixing by measuring the terms given in Eq. 7 for individual γ-ray transitions. A precise measurement of them enables us to determine all of the unknown factors contained in the terms in Eq. 7, and to study the validity of the theory based on the interference between s- and p-wave amplitudes by examining whether the theory can explain experimental values

[10] $D_0 \leq 20eV$ for uranium and thorium.

[11] In heavy nuclei, many p-wave resonances exist in slow-neutron capture reaction. In this case, we cannot apply the two level approximation since the resonances are located too close to each other. We can extract the nuclear matrix element applying a statistical procedure even in such cases [26, 27].

consistently. Here we discuss the case of the p-wave resonance for $^{139}La(E_n = 0.734eV)$. The $A_{13}\boldsymbol{\sigma}_\gamma \cdot \hat{\boldsymbol{k}}_\gamma$ term corresponds to the circular polarization of the emitted γ-rays induced by unpolarized incident neutrons (P_γ) through the relation $P_\gamma = A_{13}\sigma_r/\sigma_{n\gamma}$. The A_{13} is related to A_9 as

$$\frac{A_9}{A_{13}} = -P(J_s J_s \frac{1}{2}\frac{1}{2} 1IF), \tag{55}$$

for single γ-ray transitions (Appendix A). If we substitute $J_s = 4$, $I = 7/2$, $F = 4$, and $\langle a_\gamma \rangle = 4.7 \pm 2.1\,\%$, we obtain $|A_{13}|_{E_n = E_p \pm \Gamma_p/2} = 38 \pm 17\,\%$. Another interesting observable is the $A_2\boldsymbol{\sigma}_n \cdot (\hat{\boldsymbol{k}}_n \times \hat{\boldsymbol{k}}_\gamma)$ term [12], which is an analyzing power for transversely polarized incident neutrons. Its value in the p-wave resonance for ^{139}La can be evaluated as

$$(A_2)_{E_n = E_p} = -\sqrt{\frac{\Gamma_s^n}{\Gamma_p^n}}\sqrt{\frac{\Gamma_{M1}}{\Gamma_{E1}}}\frac{\Gamma_p}{E_p - E_s}(-0.1250x - 0.07395y), \tag{56}$$

for the γ-ray transition of $^{140}La(4^- \to 4^-)$. We obtain

$$|A_2|_{E_n = E_p} \sim 96 \pm 43\,\%, \tag{57}$$

assuming $|x| = 1$ (Appendix A). More intense neutron beam is necessary for a precise measurement of these observables. The improvement of energy resolution of γ-ray detector is also desirable.

The neutron transmission method is one of the best way to search for T-violating effects, since we can observe T-violating effects in the weak interaction free from FSI. Bunakov, Gudkov and Yamaguchi suggested the enhancement mechanism of PNC effect is also applicable to T-violating effects [39, 63, 30]. We mention a feasibility of a TRI experiment in neutron transmission method below. Interaction between low energy incident neutrons and nuclei is described using forward scattering amplitude f which can be written in the form

$$f = A' + B'\boldsymbol{\sigma}_n \cdot \hat{\boldsymbol{I}} + C'\boldsymbol{\sigma}_n \cdot \hat{\boldsymbol{I}} + D'\boldsymbol{\sigma}_n \cdot (\hat{I} \times \hat{\boldsymbol{k}}_n). \tag{58}$$

Propagation of incident neutrons through material can be described in the framework of neutron optics for low energy incident neutrons. The incoming neutron spin state (U_i) is transformed into another one (U_f) which is given as

$$U_f = \delta U_i, \quad \delta = e^{i(n-1)\rho z}, \quad n = 1 + \frac{2}{(\hbar k_n)^2}\rho f, \tag{59}$$

after the propagation of length z in material, where ρ is the number density of target nuclei. The δ is

$$\delta = A + B\boldsymbol{\sigma}_n \cdot \hat{\boldsymbol{I}} + C\boldsymbol{\sigma}_n \cdot \hat{\boldsymbol{k}}_n + D\boldsymbol{\sigma}_n \cdot (\hat{\boldsymbol{I}} \times \hat{\boldsymbol{k}}_n), \tag{60}$$

[12] P-even T-odd. We cannot test TRI in this observable since FSI is too large.

where $A = \exp(iZA')\cos b$, $B = i \exp(iZA')B'Z(\sin b)/b$, $C = i \exp(iZA')C'Z(\sin b)/b$, $D = i \exp(iZA')D'Z(\sin b)/b$, $Z = 2\pi\rho z/(\hbar k_n)$ and $b = Z|B' + C'|$. A relation $D' = 0 \rightarrow D = 0$ holds and it is equivalent to $D \neq 0 \rightarrow D' \neq 0$. Therefore, a non-zero value of D which is to be observed in the experiment is unambiguous evidence of the existence of the T-odd correlation term D'. In the measurement, we must choose an observable in which no FSI effect is included. Two candidates have been suggested. One is a spin deteiled balance with a polarized target [35] and the other is a comparison of analyzing power and polarization with a polarized target [36]. The necessary devices for these experiments are (1) a neutron polarizer (2) a polarized target and (3) a neutron spin analyzer. We already mentioned a neutron polarizer. A polarized ^3He is a candidate for the neutron spin analyzer. The technique to polarize ^3He gas is an established one [64]. Recently, a high polarization of ^3He at $6 \sim 9 atm$ has been reported [65]. In addition, it can also be used as a detector of slow neutrons. But the technique to polarize target nuclei (lanthanum etc.) is not yet established.

Dynamic nuclear polarization has been studied for lanthanum trifluoride single crystals in which neodymium ions are diluted ($La_{1-x}Nd_xF_3$ [66]). Approximately 1 % of ^{139}La polarization has been obtained for $x = 0.08$ % [47].

Neutron spins rotate due to a pseudomagnetic field [67] on propagating through a polarized target. If incident neutron spins rotate on the transmission, an experimental efficiency for a $\boldsymbol{\sigma}_n \cdot (\hat{I} \times \hat{k}_n)$ term is suppressed. The pseudomagnetic rotation can be cancelled by applying a magnetic field antiparallel to the pseudomagnetic field in a spin frozen polarized target. But the coupling energy between a nuclear quadrupole moment of ^{139}La and an electric field gradient of a lanthanum trifluoride crystal causes the overlapping of Zeeman splitting levels in the cancellation field ($\leq 2kG$) [68], and the vector polarization decreases. We must overcome the problem. Single crystals of La_2O_3, $LaAlO_3$, La_2O_2S, KBr etc. have high symmetries and quadrupole couplings are diagonalized about their c-axes. Currently, g-factors of neodymium ions diluted in these crystals are being studied.

An experimental accuracy of 10^{-2} to 10^{-3} is expected for the size of a P-odd T-odd amplitude relative to a P-odd T-even one, if we can polarize ^{139}La nuclei more than 20 %. The accuracy can be improved up to 10^{-4} with higher nuclear polarization, precise control of magnetic field and more intense neutron beam.

Acknowledgements

The author would like to thank Prof. A. Masaike for the careful advice, helpful discussion and collaboration. He thanks Profs. K. Imai and H. En'yo for their advice and helpful discussions. He thanks Drs. T. Adachi, S. Ishimoto, Y. Masuda, Prof. K. Morimoto and Ms. Y. Morishita for their collaboration and valuable discussions. He also thanks Profs. C. D. Bowman, J. D. Bowman, C. R. Gould, V. P. Gudkov, S. Penttilä and S. J. Seestrom for their valuable discussions. He thanks all the staff members at KEK who have constructed, maintained and operated

the neutron spallation source. The author gratefully acknowledges Prof. F. Okamura for the kind help in the crystallography, Prof. Y. Uchida for the kind help in ESR study of lanthanum trifluoride crystal and Dr. Y. Takahashi for the valuable discussions on single crystals of lanthanum compounds.

Finally, the author would like to thank all his family, especially his wife for their great support throughout his studies.

References

[1] T. D. Lee and C. N. Yang, Phys. Rev. **104**, 254 (1956).
[2] C. S. Wu et al., Phys. Rev. **105**, 1413 (1957).
[3] D. H. Wilkinson, Phys. Rev. **109**, 1603 (1958).
[4] R. J. Blin-Stoyle, Phys. Rev. **118**, 1605 (1960).
[5] D. E. Nagel et al., High Energy Physics with Polarized Beams and Targets, ed. G. H. Thomas, AIP Conference Proceedings No. 51, (American Institute of Physics, New York, 1978), p. 224.
[6] R. Balzer et al., Phys. Rev. **C30**, 1409 (1984).
[7] P. von Rossen et al., Polarization Phenomena in Nuclear Physics, 1980, Santa Fe, eds. D. E. Nagle et al., AIP Conference Proceedings No. 69, (American Institute of Physics, New York, 1981), p. 1442.
[8] V. Yuan et al., Phys. Rev. Lett. **57**, 1680 (1986).
[9] Yu. G. Abov et al., Phys. Lett. **12**, 25 (1964).
[10] J. L. Alberi et al., Phys. Rev. Lett. **29**, 518 (1972).
[11] J. F. Cavignac et al., Phys. Lett. **B67**, 148 (1977).
[12] V. M. Lobashov et al., Nucl. Phys. **A197**, 241 (1972).
[13] C. A. Barnes et al., Unification of Elementary Forces and Gauge Theory, eds. D. Cline and F. Mills, (Harwood, London, 1978), p. 235.
[14] E. G. Adelberger et al., Phys. Rev. Lett. **34** 402 (1975).
[15] V. M. Lobashov et al., Yad. Fiz. **15** 1142 (1972) [Sov. J. Nucl. Phys. **15** 1142 (1972)].
[16] H. Benkoula et al., Phys. Lett. **B71** 287 (1977).
[17] G. V. Danilyan et al., Pis'ma Zh. Eksp. Teor. Fiz. **24** 380 (1976) [JETP Lett. **24** 344 (1976)].
[18] E. Kuphal et al., Nucl. Phys. **A234** 380 (1976) [JETP Lett. **24** 344 (1976)].
[19] P. Jenschke and P. Bock, Phys. Lett. **B31** 65 (1970), E. D. Lipson et al., Phys. Lett. **B35** 307 (1971).
[20] K. S. Krane et al., Phys. Rev. **C5** 1663 (1972).
[21] S. W. Herb et al., Phys. Rev. Lett. **39** 252 (1977).
[22] M. Forte et al., Phys. Rev. Lett. **45** 2088 (1980).
[23] V. P. Alfimenkov et al., Nucl. Phys. **A398**, 93 (1983).
[24] S. A. Biryukov et al., Yad. Fiz. **45**, 1511 (1987) [Sov. J. Nucl. Phys. **45** 937 (1987)].
[25] Y. Masuda et al., Nucl. Phys. **A478**, 737c (1988), Nucl. Phys. **A504**, 269 (1989).
[26] J. D. Bowman et al., Phys. Rev. Lett. **65**, 1192 (1990).
[27] C. M. Frankle et al., Phys. Rev. Lett. **67**, 564 (1991).
[28] V. Yuan et al., (to be published).
[29] O. P. Sushkov and V. V. Flambaum, Usp. Fiz. Nauk. **136** 2 (1982) [Sov. Phys. Usp. **25** 1 (1982)].
[30] Y. Yamaguchi, J. Phys. Soc. Jpn. **57** 1518(L) (1988); ibid 1522(L); ibid 1525(L); ibid 2331; ibid 3339; ibid 3344.
[31] Y. Yamaguchi, Prog. Theor. Phys. **85** 101 (1991), N. Ishikawa, Master thesis submitted to Tokai Univ. (unpublished, in Japanese).
[32] L. Stodolsky, Nucl. Phys. **B197** 213 (1982).
[33] P. K. Kabir, Phys. Rev. **D25** 2013 (1982).
[34] V. E. Bunakov and V. P. Gudkov, Nucl. Phys. **A401** 93 (1983).

[35] L. Stodolsky, Phys. Lett. **172B** 5 (1986).
[36] P. K. Kabir, Phys. Rev. Lett. **60** 686 (1988).
[37] J. H. Christenson et al., Phys. Rev. Lett. **13** 138 (1964).
[38] G. Lüders, Ann. Phys. **2** 1 (1957).
[39] V. E. Bunakov and V. P. Gudkov, Test of Time Reversal Invariance in Neutron Physics, 1987. Proc. of the Aqueduct Conference Center Workshop on Tests of Time Reversal Invariance in Neutron Physics, eds. N. R. Roberson, C. R. Gould and J. D. Bowman. p. 175, World Scientific Publishing.
[40] V. P. Gudkov, KEK-Preprint-91–139.
[41] L. Stodolsky, Test of Time Reversal Invariance in Neutron Physics, 1987. Proc. of the A queduct Conference Center Workshop on Tests of Time Reversal Invariance in Neutron Physics, eds. N. R. Roberson, C. R. Gould and J. D. Bowman. p. 12, World Scientific Publishing.
[42] A. Hallin et al., Phys. Rev. Lett. **52**, 337 (1984).
[43] C. G. Callan et al., Phys. Rev. **162**, 1494 (1967).
[44] D. Thompson et al., Nucl. Inst. Meth. **A284**, 40 (1989).
[45] I. S. Altarev et al., Pis'ma Zh. Eksp. Teor. Fiz. **44** 360 (1986) [JETP Lett. **44**, 460 (1986)].
[46] J. R. Vanhoy et al., Z. Phys. **A331** (1988) 1
[47] Y. Masuda et al., 18th INS International Symposium on Physics with High-Intensity Hadron Accelerators, Tokyo, March 14–16, 1990.
[48] V. V. Flambaum and O. P. Sushkov, Nucl. Phys. **A435**, 352 (1985).
[49] N. Watanabe et al., 9th Meeting of International Collaboration on Advanced Neutron Sources (ICANS-IX), SIN, Villingen, Switzerland. September 22–26, 1986.; N. Watanabe, 10th Meeting of International Collaboration on A dvanced Neutron Sources (ICANS-IX), Los Alamos, New Mexico, U.S.A. October 3–7, 1988.
[50] H. Rauh and N. Watanabe, Nucl. Inst. Meth. **222** 507 (1984).
[51] H. M. Shimizu et al., 11th Meeting of International Collaboration on Advanced Neutron Sources (ICANS-XI), KEK, Tsukuba, Japan. October 22–26, 1990.
[52] Y. Masuda et al., Nucl. Inst. Math. **A264** 169 (1988).
[53] W. de Boer et al., Phys. Rev. **B12** 847 (1975), W. de Boer, CERN 74–11, Laboratory I, Nuclear Physics Division (1974).
[54] V. I. Lushchikov et al., Yad. Fiz. **10**, 669 (1969) [Sov. J. Nucl. Phys. **10** 669 (1970)].
[55] S. Hiramatsu et al., J. Phys. Soc. Jpn. **45**, 949 (1978).
[56] N. Hoshizaki and A. Masaike, Jpn. J. App. Phys. **25**, L244 (1986).
[57] S. Ishimoto et al., Jpn. J. App. Phys. **25**, L246 (1986).
[58] H. Kobayashi et al., Nucl. Inst. Meth. **A270**, 106 (1988).
[59] L. B. Hughes et al., Nucl. Phys. **89**, 241 (1966).
[60] L. V. Groshev et al., Nuclear Data Tables **A5**, 1 (1968).
[61] R. M. Moon et al., Phys. Rev. **181**, 920 (1969).
[62] S. F. Mughabghab et al., Neutron Cross Sections (Academic Press, New York, 1981).
[63] V. E. Bunakov and V. P. Gudkov, Z. Phys. **A308**, 363 (1982).
[64] K. P. Coulter et al., Test of Time Reversal Invariance in Neutron Physics, 1987. Proc. of the Aqueduct Conference Center Workshop on Tests of Time Reversal Invariance in Neutron Physics, eds. N. R. Roberson, C. R. Gould and J. D. Bowman. p. 140, World Scientific Publishing.
[65] O. Häusser et al., 4th Conference on the Intersections between Particles and Nuclear Physics, Tucson, May 24–29, 1991.
[66] M. B. Shultz and C. D. Jeffries, Phys. Rev. **149** 270 (1966).
[67] H. Glättli, J. de Phys. **40** 629 (1979).
[68] K. Lee et al., Phys. Rev. **150** 168 (1966).

Appendix A Details of the Formalism of $(\vec{n}, \gamma)$ Reaction Cross Section

In this section, we describe explicit expressions of angular and polarization dependent terms which appear in section 2 and important relations between them. The case of single γ-ray transition is described here.

Intrinsic parity of a final state of a γ-ray transition is assumed to be the same as that of a compound state. The dominant parity favored transition is an M1 transition while the dominant parity unfavored one is E1.

$$a_0 = \sum_{J_s} |V_1(J_s)|^2 + \sum_{J_p j} |V_2(J_p j)|^2 \tag{A-1a}$$

$$a_1 = 2Re \sum_{J_s J_p j} V_1(J_s) V_2^*(J_p j) P(J_s J_p \tfrac{1}{2} j 1 I F) \tag{A-1b}$$

$$a_3 = Re \sum_{J_p j J'_p j'} 3\sqrt{10}\, V_2(J_p j) V_2^*(J'_p j') P(J_p J'_p j j' 2 I F) \begin{Bmatrix} 2 & 1 & 1 \\ 0 & \frac{1}{2} & \frac{1}{2} \\ 2 & j & j' \end{Bmatrix} \tag{A-1c}$$

$$\begin{aligned} a_9 = & -2Re \sum_{J_s J'_s} V_1(J_s) V_3^*(J'_s) P(J_s J'_s \tfrac{1}{2} \tfrac{1}{2} 1 I F) \\ & + \sum_{J_p j J'_p j'} V_2(J_p j) V_4^*(J'_p j') P(J_p J'_p j j' 1 I F) 6 \begin{Bmatrix} 0 & 1 & 1 \\ 1 & \frac{1}{2} & \frac{1}{2} \\ 1 & j & j' \end{Bmatrix} \end{aligned} \tag{A-1d}$$

$$a_{10} = -2Re \sum_{J_s} \left(V_2(J_p = J_s, \tfrac{1}{2}) V_3^*(J_s) + V_1(J_s) V_4^*(J_p = J_s, \tfrac{1}{2}) \right) \tag{A-1e}$$

$$a_{11} = Re \sum_{J_s J_p} \left(V_2(J_p, \tfrac{3}{2}) V_3^*(J_s) + V_1(J_s) V_4^*(J_p, \tfrac{3}{2}) \right) \sqrt{3}\, P(J_s J_p \tfrac{1}{2} \tfrac{3}{2} 2 I F) \tag{A-1f}$$

$$a_{12} = -2Re \sum_{J_p j J'_p j'} V_2(J_p j) V_4^*(J'_p j') P(J_p J'_p j j' 1 I F) 18 \begin{Bmatrix} 2 & 1 & 1 \\ 1 & \frac{1}{2} & \frac{1}{2} \\ 1 & j & j' \end{Bmatrix} \tag{A-1g}$$

The I, J_s, J_p and F are spins of target nucleus, s-wave resonance, p-wave resonance and final state, respectively. The j is the total angular momentum of the incident neutron ($j = \frac{1}{2}$ or $\frac{3}{2}$). The V_i's are the invariant amplitudes defined as

$$V_1 = -\frac{1}{2k} \frac{\sqrt{3}}{2} \frac{T_s A_{M1}(1+\alpha)}{E_n - E_s + \frac{i}{2}\Gamma_s}, \tag{A-2a}$$

$$V_2(j) = -\frac{1}{2k}\frac{\sqrt{3}}{2}\frac{T_p(j)A_{E1}}{E_n - E_p + \frac{i}{2}\Gamma_p}, \tag{A-2b}$$

$$V_3 = -\frac{1}{2k}\frac{\sqrt{3}}{2}\frac{T_s W A_{E1}(1+\beta)}{\left(E_n - E_p + \frac{i}{2}\Gamma_p\right)\left(E_n - E_s + \frac{i}{2}\Gamma_s\right)}, \tag{A-2c}$$

$$V_4(j) = -\frac{1}{2k}\frac{\sqrt{3}}{2}\frac{T_p(j) W A_{M1}(1+\gamma)}{\left(E_n - E_s + \frac{i}{2}\Gamma_s\right)\left(E_n - E_p + \frac{i}{2}\Gamma_p\right)}, \tag{A-2d}$$

where $T_s = \eta_s\sqrt{\Gamma_s^n(E_n)}$, $T_p(j) = \eta_{pj}\sqrt{\Gamma_{pj}^n(E_n)}$, $A_{M1(E1)} = \eta_\gamma\sqrt{\Gamma_{M1(E1)}}$. The α, β and γ represent contributions of far s-wave resonances. They are zero if only one s-wave resonance contributes. Corresponding diagrams are shown in Fig. 21. The η's are phase factors and almost equal to ± 1 in low energy neutron capture reactions [48]. The T_s and $T_p(j)$ are reduced T-matrix elements for s-wave resonance and p-wave resonance. The A_{M1} and A_{E1} are reduced T-matrix elements for parity-favored and parity-unfavored γ-ray transitions. The E_n is the incident neutron energy. The E_s and E_p are resonance energies of s- and p-wave resonances. The Γ_s and Γ_p are resonance widths of s- and p-wave resonances. The Γ_s^n and Γ_p^n are neutron widths of s- and p-wave resonances. The Γ_{M1} and Γ_{E1} are widths of parity-favored and parity-unfavored γ-ray transitions. The function P is given in Eq. 51. We discuss the magnitude of a_i relative to a p-wave resonance

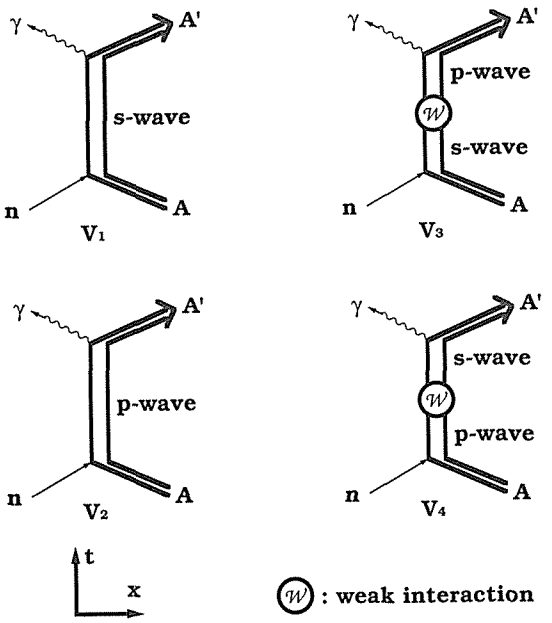

Fig. 21. The diagrams of invariant amplitudes [48].

cross section [13].

$$A_i = \frac{a_i}{a_{0p}} \tag{A-3}$$

The a_{0p} is given as $a_{0p} = \Sigma_j |V_2(J_p j)|^2$. This definition is useful only in the vicinity of the p-wave resonance. If we go far from the p-wave resonance, the denominator in Eq. A–3 becomes too small. If we assume that only one s-wave resonance exist close to the p-wave resonance, we obtain

$$A_1 = \eta_\gamma \frac{1}{(E_n - E_s)^2 + \frac{\Gamma_s^2}{4}} \sqrt{\frac{\Gamma_s^n}{\Gamma_p^n}\frac{\Gamma_{M1}}{\Gamma_{E1}}} \left((E_n - E_p)(E_n - E_s) + \frac{\Gamma_s \Gamma_p}{4} \right) \times \sum_j \xi_j P\left(J_s J_p \frac{1}{2} j 1 IF\right) \tag{A-4a}$$

$$A_3 = 3\sqrt{10} \sum_{jj'} \xi_j \xi_{j'} P(J_p J_p j j' 2 IF) \begin{Bmatrix} 2 & 1 & 1 \\ 0 & \frac{1}{2} & \frac{1}{2} \\ 2 & j & j' \end{Bmatrix} \tag{A-4b}$$

$$A_9 = -2\eta_\gamma \frac{W}{(E_n - E_s)^2 + \frac{\Gamma_s^2}{4}} \frac{\Gamma_s^n}{\Gamma_p^n} \sqrt{\frac{\Gamma_{M1}}{\Gamma_{E1}}} \left((E_n - E_p) P\left(J_s J_s \frac{1}{2} \frac{1}{2} 1 IF\right) + 6(E_n - E_s) \frac{\Gamma_p^n}{\Gamma_s^n} \sum_{jj'} \xi_j \xi_{j'} P(J_p J_p j j' 1 IF) \begin{Bmatrix} 0 & 1 & 1 \\ 1 & \frac{1}{2} & \frac{1}{2} \\ 1 & j & j' \end{Bmatrix} \right) \tag{A-4c}$$

$$A_{10} = -2x \frac{W}{(E_n - E_s)^2 + \frac{\Gamma_s^2}{4}} \sqrt{\frac{\Gamma_s^n}{\Gamma_p^n}} \left((E_n - E_s) + (E - E_p) \frac{\Gamma_{M1}}{\Gamma_{E1}} \right) \tag{A-4d}$$

$$A_{11} = \sqrt{3} y \frac{W}{(E_n - E_s)^2 + \frac{\Gamma_s^2}{4}} \sqrt{\frac{\Gamma_s^n}{\Gamma_p^n}} \left((E_n - E_s) + (E_n - E_p) \frac{\Gamma_{M1}}{\Gamma_{E1}} \right) P\left(J_s J_p \frac{1}{2} \frac{3}{2} 2 IF\right). \tag{A-4e}$$

$$A_{12} = -36\eta_\gamma \frac{W}{(E_n - E_s)^2 + \frac{\Gamma_s^2}{4}} \sqrt{\frac{\Gamma_{M1}}{\Gamma_{E1}}} (E_n - E_s) \sum_{jj'} \xi_j \xi_{j'} P(J_p J_p j j' 1 IF) \begin{Bmatrix} 2 & 1 & 1 \\ 1 & \frac{1}{2} & \frac{1}{2} \\ 1 & j & j' \end{Bmatrix} \tag{A-4f}$$

[13] The A_i's are defined as $A_i = a_i/a_0$ in Ref. [48].

The following relations typically hold for incident epithermal neutrons.

$$\Gamma_s, \Gamma_p \ll E_p - E_s, \quad \sqrt{\frac{\Gamma_s^n}{\Gamma_p^n}} \simeq 10^3, \quad \sqrt{\frac{\Gamma_{M1}}{\Gamma_{E1}}} \simeq 10^{-2} \sim 10^2 \tag{A-5}$$

We can omit A_{12} in the vicinity of the p-wave resonance, since its contribution is $\Gamma_p^n/\Gamma_s^n(\sim 10^{-6})$ times smaller than that of A_9.

We discuss the case of the p-wave resonance for ^{139}La ($E_n = 0.734eV$) below. We take the s-wave resonance at $E_n = -48.63eV$ as the neighboring s-wave resonance since it is the nearest to the p-wave resonance. The ground state of ^{139}La has $I^\pi = 7/2^+$. The neutron orbital angular momentum is $l = 1$. The dominant γ-ray transition near Q-value is the transition into the state of $F^\pi = 4^-$ of ^{140}La [59, 60]. Therefore, the allowed γ-ray transition is $M1$ and forbidden one is $E1$. Substituting $I = 7/2$, $J_s = 4$, $J_p = 4$ and $F = 4$ and $F = 4$ into Eq. A–4, we obtain the following relations.

$$A_1 \sim \eta_\gamma(-0.1250x + 0.1479y)\frac{1}{(E_p - E_s)}\sqrt{\frac{\Gamma_s^n}{\Gamma_p^n}\frac{\Gamma_{M1}}{\Gamma_{E1}}}(E_n - E_p) \tag{A-6a}$$

$$A_3 = 3\sqrt{10}(0.1029xy - 0.0174y^2) \tag{A-6a}$$

$$A_9 \sim -2 \times (-0.1250)\eta_\gamma \frac{W}{(E_p - E_s)^2}\frac{\Gamma_s^n}{\Gamma_p^n}\sqrt{\frac{\Gamma_{M1}}{\Gamma_{E1}}}(E_n - E_p) \tag{A-6c}$$

$$A_{10} \sim -2x\frac{W}{E_p - E_s}\sqrt{\frac{\Gamma_s^n}{\Gamma_p^n}} \tag{A-6d}$$

$$A_{11} \sim \sqrt{3}(-0.5636y)\frac{W}{E_p - E_s}\sqrt{\frac{\Gamma_s^n}{\Gamma_p^n}} \tag{A-6e}$$

Other important terms in Eq. 7 are $a_2\boldsymbol{\sigma}_n \cdot (\hat{\boldsymbol{k}}_n \times \hat{\boldsymbol{k}}_\gamma)$ and $a_{13}\boldsymbol{\sigma}_\gamma \cdot \hat{\boldsymbol{k}}_\gamma$. The a_2 corresponds to an analyzing power for transversely polarized incident neutrons, while a_{13} is related to an circular polarization of emitted γ-rays induced by unpolarized incident neutrons (P_γ). Their explicit expressions are given as

$$a_2 = -2Im\sum_{J_sJ_pj} V_1(J_s)V_2^*(J_pj)\beta_j P(J_sJ_p\frac{1}{2}j1IF), \tag{A-7a}$$

$$a_{13} = 2Re(\sum_{J_s} V_1(J_s)V_3^*(J_s) + \sum_{J_pj} V_2(J_pj)V_4^*(J_pj)), \tag{A-7b}$$

where

$$\beta_j = \begin{cases} 1, & j = \frac{1}{2}, \\ -\frac{1}{2}, & j = \frac{3}{2}. \end{cases} \tag{A-8}$$

If we divide them by a_{0p}, we obtain

$$A_2 = -\eta_\gamma \sqrt{\frac{\Gamma_s^n}{\Gamma_p^n}} \sqrt{\frac{\Gamma_{M1}}{\Gamma_{E1}}} \frac{\Gamma_p}{(E_p - E_s)^2} \left((E_n - E_s) - \frac{\Gamma_s}{\Gamma_p}(E_n - E_p) \right) \times \sum_j \xi_j \beta_j P(J_s J_p \frac{1}{2} j 1 I F), \tag{A-9a}$$

$$A_{13} \sim 2\eta_\gamma \frac{W}{(E_p - E_s)^2} \sqrt{\frac{\Gamma_{M1}}{\Gamma_{E1}}} \frac{\Gamma_s^n}{\Gamma_p^n}(E_n - E_p). \tag{A-9b}$$

The following relations are important.

$$\frac{A_9}{A_{13}} = -P(J_s J_s \frac{1}{2} \frac{1}{2} 1 I F) \tag{A-10a}$$

$$(A_2)_{E_n = E_p} = -\eta_\gamma \sqrt{\frac{\Gamma_s^n}{\Gamma_p^n}} \sqrt{\frac{\Gamma_{M1}}{\Gamma_{E1}}} \frac{\Gamma_p}{E_p - E_s} \sum_j \xi_j \beta_j P(J_s J_p \frac{1}{2} j 1 I F) \tag{A-10b}$$

Substituting $I = 7/2$, $J_s = 4$, $J_p = 4$ and $F = 4$ into Eq. A–10, we obtain the following relations.

$$\frac{A_9}{A_{13}} = 0.1250 \tag{A-11a}$$

$$(A_2)_{E_n = E_p} = -\eta_\gamma \sqrt{\frac{\Gamma_s^n}{\Gamma_p^n}} \sqrt{\frac{\Gamma_{M1}}{\Gamma_{E1}}} \frac{\Gamma_p}{E_p - E_s} (-0.1250x - 0.07395y) \tag{A-11b}$$

Appendix B Dynamic Polarization

Dynamic polarization is a well established method to obtain a large nuclear polarization by pumping nuclear spins in a material applying a microwave which resonates paramagnetic centers. An overview of the principle of dynamic polarization is discussed in this section. We write spins of electron and nucleus as $\boldsymbol{s}$ and $\boldsymbol{I}$, respectively.

For simplicity, we discuss only the system which consists of paramagnetic centers and one kind of nuclei of $I = 1/2$. The total hamiltonian of the spin system in a magnetic field is given as

$$H = H_{sz} + H_{Iz} + H_{ss} + H_{II} + H_{sI} + H_{RF}, \tag{B-1}$$

where a spin-lattice interaction is ignored. The first and second terms represent the Zeeman energy terms of electron and nucleus. The third, fourth and fifth terms represent spin-spin interactions between electrons, nuclei and electron-nucleus. The last term is a possible effect of oscillating magnetic field of the applied microwave. We discuss the simplest case in which only one electron and one proton are included. The H_Z given as $H_Z = H_{sz} + H_{Iz} + H_{sI} + H_{RF}$ is diagonal when we take a state vector of this system as $|s_z, I_z\rangle$ with a quantization axis

which is parallel to the direction of the applied magnetic field. When we denote magnetic substates of $\pm 1/2$ as $\pm$, each state satisfies the following relations.

$$\begin{cases} H_z|+-\rangle = \quad (E_s + E_I)|+-\rangle, \\ H_z|++\rangle = \quad (E_s - E_I)|++\rangle, \\ H_z|--\rangle = (-E_s + E_I)|--\rangle, \\ H_z|-+\rangle = (-E_s - E_I)|-+\rangle. \end{cases} \tag{B-2}$$

Off-diagonal components are included in H_{sI}. They can be evaluated in the first order perturbation as

$$\begin{cases} |a\rangle = |-+\rangle + \varepsilon^*|--\rangle, \\ |b\rangle = |--\rangle + \varepsilon\ |-+\rangle, \\ |c\rangle = |++\rangle + \varepsilon^*|+-\rangle, \\ |d\rangle = |+-\rangle + \varepsilon\ |++\rangle. \end{cases} \tag{B-3}$$

When H_{sI} is assumed to be the dipole interaction as

$$H_{sI} = \frac{\hbar^2 \gamma_e \gamma_I}{r^3}\left(\boldsymbol{s}\cdot\boldsymbol{I} - \frac{3(\boldsymbol{s}\cdot\boldsymbol{r})(\boldsymbol{I}\cdot\boldsymbol{r})}{r^2}\right), \tag{B-4}$$

the ε is given as

$$\varepsilon = \frac{3}{4}\frac{\hbar\gamma_e}{r^3 H_0}\sin\theta\cos\theta e^{-i\phi}, \tag{B-5}$$

where the H_0 is the magnitude of external magnetic field, and θ and ϕ are spherical angles of the vector $\boldsymbol{r}$ which connects the electron and proton. Transitions of $|a\rangle \leftrightarrow |c\rangle$ and $|b\rangle \leftrightarrow |d\rangle$ are allowed transitions. When the microwave is applied at $\nu_0 (= 2E_s/h)$, strong electron spin resonance (ESR) is observed. Transitions of $|a\rangle \leftrightarrow |d\rangle$ and $|b\rangle \leftrightarrow |c\rangle$ are forbidden transitions. The microwave of $\nu = \nu_0 \pm \Delta\nu (= 2(E_s \pm E_S)/h)$ induces a weak electron spin resonance corresponding to the forbidden transition. The probability of the forbidden transition is known to be $4|\varepsilon|^2$ times that of allowed transition by evaluating a matrix element of H_{RF} between two admixed states [53].

The population of the states $|a\rangle, |b\rangle, |c\rangle, |d\rangle$ obey the Boltzmann distribution when no microwave is applied. A polarization p of a particle whose spin is J is given as

$$p = \frac{1}{J}\frac{\sum_{m=-J}^{J} mN_m}{\sum_{m=-J}^{J} N_m}, \tag{B-6}$$

where N_m is population of a magnetic substate. The population is given as

$$N_m \propto e^{-\frac{m\hbar\gamma H_0}{kT}}. \tag{B-7}$$

The polarization p is given as

$$p = \frac{2J+1}{2J} \coth\left(\frac{2J+1}{2J}\frac{\mu H_0}{kT}\right) - \frac{1}{2J}\coth\left(\frac{1}{2J}\frac{\mu H_0}{kT}\right). \tag{B-8}$$

The polarization of a free electron is $-99.75\,\%$ with a $25kG$ magnetic field at $0.5K$ while the polarization of a proton is only $0.51\,\%$.

In a dynamic polarization, a microwave is applied at $\nu = \nu_0 \pm \Delta\nu$. Let us consider the case of $\nu = \nu_0 - \Delta\nu$. If no microwave is applied, the electron-proton system stays in the lowest energy state, namely $|a\rangle$, with a large probability which is determined by a thermal equilibrium. The microwave induces a forbidden transition between $|b\rangle \leftrightarrow |c\rangle$. The double spin-flip transition pushes up the state to higher energy state. The electron spin is flipped to the original spin direction through a spin-lattice relaxation typically within the time of the order of *msec*, while proton spin is flipped very slowly within the time of the order of *sec*. The large difference between these two relaxation times causes a net transition of

$$|b\rangle \longrightarrow |c\rangle \longrightarrow |a\rangle.$$

The interaction which is responsible for the double spin-flip transition is the dipole interaction included in H_{sI}. The probability of the forbidden transition is proportional to $|\varepsilon|^2 \propto r^{-6}$. Therefore only the neighboring nuclei around a radical electron are polarized through this mechanism. The nuclear polarization is transferred to remote nuclei through spin-spin coupling ($I^i_{\pm} I^j_{\mp}$). This mechanism is referred to as "spin diffusion". The characteristic time for spin diffusion is order of *sec*. The "spin diffusion" works well when two nuclear spins have an identical magnetic moment and magnitude of spin. Finally we can obtain a very high polarization in a material uniformly.

When a microwave frequency is set at $\nu = \nu_0 + \Delta\nu$, the net transition of

$$|a\rangle \longrightarrow |d\rangle \longrightarrow |b\rangle.$$

is enhanced. Then a negative nuclear polarization is obtained.

Both positive- and negative-nuclear polarization can be obtained by choosing the microwave frequency with a fixed magnetic field.

Appendix C T-violating Observables in Neutron Transmission

We describe T-violating observables in a low-energy neutron transmission experiment below [35, 36]. In Eq. 60, we assume the $\boldsymbol{\sigma}_n$, $\hat{\boldsymbol{I}}$ and $\hat{\boldsymbol{k}}_n$ are perpendicular to each other and $\boldsymbol{\sigma}_n // x$, $\hat{\boldsymbol{I}} // y$ and $\hat{\boldsymbol{k}}_n // z$. When we write

$$\boldsymbol{E} = B\hat{\boldsymbol{I}} + C\hat{\boldsymbol{k}}_n + D\hat{\boldsymbol{I}} \times \hat{\boldsymbol{k}}_n = \begin{pmatrix} B \\ D \\ C \end{pmatrix}, \tag{C-1}$$

the δ can be written as

$$\delta = A + \boldsymbol{\sigma}_n \cdot \boldsymbol{E}. \tag{C-2}$$

An analyzing power and a polarization vector in this process, which are represented by $\boldsymbol{A}$ and $\boldsymbol{P}$, respectively, are given as

$$\mathbf{A} = Tr(\delta^\dagger \boldsymbol{\sigma}_n \delta) = 4 ReA^* \mathbf{E} - 2i \mathbf{E}^* \times \mathbf{E}, \tag{C-3a}$$

$$\mathbf{P} = Tr(\boldsymbol{\sigma}_n \delta^\dagger \delta) = 4 ReA^* \mathbf{E} + 2i \mathbf{E}^* \times \mathbf{E}. \tag{C-3b}$$

Therefore, the following relations are obtained.

$$\mathbf{A} + \mathbf{P} = 8 ReA^* \mathbf{E} = 8 \begin{pmatrix} ReA^* B \\ ReA^* D \\ ReA^* C \end{pmatrix} \tag{C-4a}$$

$$\mathbf{A} - \mathbf{P} = -4i \mathbf{E}^* \times \mathbf{E} = 4 \begin{pmatrix} -ImC^* D \\ -ImB^* C \\ ImB^* D \end{pmatrix} \tag{C-4b}$$

The $(A + P)_y$, $(A - P)_x$ and $(A - P)_z$ are proportional to D which signals T-violation. It is natural to assume that the magnitude of A is biggest among those of A, B, C and D. The $(A + P)_y$ is expected to be the biggest T-violating observable among them.

In a similar way, we can find other observables which are sensitive to T-violation. We use $Prob(i \to j)$ to represent the expectation value of the transmitted neutron polarization in the direction j with 100 % polarized incident neutrons in the direction i.

$$\begin{aligned} Prob(i \longrightarrow j) &= Tr\left(\frac{1 + (\boldsymbol{\sigma}_n)_j}{2} \delta^\dagger \frac{1 + (\boldsymbol{\sigma}_n)_i}{2} \delta \right) \\ &= \frac{1 + \delta_{ij}}{2} |A|^2 + \frac{1 - \delta_{ij}}{2} |\mathbf{E}|^2 \\ &\quad + ReA^*(E_i + E_j) + i \sum_{kl} \frac{\varepsilon_{ikl} - \varepsilon_{jkl}}{2} E_k^* E_l + Re E_i^* E_j \\ &\quad + \sum_k \varepsilon_{ijk} ImA^* E_k \end{aligned} \tag{C-5}$$

The δ_{ij} and ε_{ijk} are given as follows.

$$\delta_{ij} = \begin{cases} 1 & (i = j) \\ 0 & (i \neq j) \end{cases} \tag{C-6}$$

$$\varepsilon_{ijk} = \begin{cases} 1 & \text{(if } ijk \text{ is an even permutation of 123)} \\ -1 & \text{(if } ijk \text{ is an odd permutation of 123)} \\ 0 & \text{(otherwise)} \end{cases} \tag{C-7}$$

We find several observables which are proportional to D among the following observables.

$$Prob(+i \to -i) - Prob(-i \to +i) = -2i(\mathbf{E}^* \times \mathbf{E})_i = 4 \begin{pmatrix} ImC^*D \\ ImB^*C \\ ImB^*D \end{pmatrix} \tag{C-8a}$$

$$Prob(+i \to +i) - Prob(-i \to -i) = 4ReA^*E_i = 4 \begin{pmatrix} ImA^*B \\ ImA^*D \\ ImA^*C \end{pmatrix} \tag{C-8b}$$

Those are $Prob(+x \to -x) - Prob(-x \to +x)$, $Prob(+y \to +y) - Prob(-y \to -y)$ and $Prob(+z \to -z) - Prob(-z \to +z)$.

Appendix D Numerical Simulation

The $N_i(p_n, A_L)$ (Eq. 29) depends on the energy of incident neutrons, so does $N(p_n, A_L)$. The E_n dependence of resonance cross section obtained in experiment was used to include the effect of Doppler broadening as a spreading of resonance width. The N_i's were calculated as

$$N_0(p_n, A_L) = \int d\Omega \int_{V_B} \frac{d^3r}{S_B} e^{-nX_t z} n \frac{dX_r}{d\Omega} = \frac{X_r}{X_t}(1 - e^{nX_t t}),$$

$$N_1(p_n, A_L) = \int dE_1 \int d\Omega_1 \int_{V_B} \frac{d^3r_1}{S_B} e^{-nX_t z_1} n \frac{d\sigma_{sc}}{d\Omega_1} \kappa(E_1, E_n; \hat{k}_n, \vec{\Omega}_1) \frac{X_r}{X_t}(1 - e^{nX_t \ell(\vec{r}_1, \vec{\Omega}_1)}),$$

$$N_2(p_n, A_L) = \int dE_2 \int dE_1 \int d\Omega_2 \int_{V_B} \frac{d^3r_1}{S_B} \int_V \frac{d^3r_2}{S} e^{-nX_t z_1} n \frac{d\sigma_{sc}}{d\Omega_{12}} \kappa(E_1, E_2; \hat{k}_n, \hat{\vec{r}}_{12})$$

$$\times e^{-nX_t |\vec{r}_{12}|} n \frac{d\sigma_{sc}}{d\Omega_2} \kappa(E_2, E_n; \hat{\vec{r}}_{12}, \vec{\Omega}_2) \frac{X_r}{X_t}(1 - e^{nX_t \ell(\vec{r}_2, \vec{\Omega}_2)}),$$

$$\vdots \tag{D-1}$$

where

$$X_t = \sigma_{sc} + \sigma_c(E_n) + X_r,$$

$$X_r = \sigma_r(E_n) \times \left((1 + A_L)\frac{(1 + p_n)}{2} + (1 - A_L)\frac{(1 - p_n)}{2} \right),$$

$$\vec{r}_{12} = \vec{r}_2 - \vec{r}_1, \quad \hat{\vec{r}}_{12} = \frac{\vec{r}_2 - \vec{r}_1}{|\vec{r}_2 - \vec{r}_1|},$$

and

E_n	:	incident neutron energy,
p_n	:	longitudinal polarization of incident neutron,
A_L	:	longitudinal asymmetry,
σ_{sc}	:	potential scattering cross section,
σ_c	:	continuum part of capture cross section,
σ_r	:	resonance part of capture cross section,
n	:	number density of target nuclei,
V	:	target volume,
V_B	:	intersection between target volume and incident beam,
S	:	cross section of V,
S_B	:	cross section of V_B,
$\ell(\vec{r}, \vec{\Omega})$	:	target thickness for the neutron which is scattered at the point $\vec{r}$ and propagated parallel to $\vec{\Omega}$.

The function κ is unity only when arguments are allowed in elastic scattering kinematically, otherwise it is zero. The $\vec{\Omega}, \vec{\Omega}_1, \vec{\Omega}_2, \ldots$ are unit vector variables which run over whole solid angle. The Ω_{12} is the solid angle of the volume d^3r_2 seen from the point $\vec{r}_1$.